Epigenetic modifications regulate cultivar-specific root development and metabolic adaptation to nitrogen availability in wheat

Jun Xiao (jxiao@genetics.ac.cn)
Institute of Genetics and Developmental Biology, Chinese Academy of Sciences https://orcid.org/0000-0002-6077-2155

Hao Zhang
Institute of Genetics and Developmental Biology, Chinese Academy of Sciences

Zhiyuan Jin
College of Life Sciences, Hebei Normal University

Fa Cui
College of Agriculture, Ludong University

Long Zhao

Xiaoyu Zhang
Institute of Genetics and Developmental Biology, Chinese Academy of Sciences

Jinchao Chen
Institute of Genetics and Developmental Biology, Chinese Academy of Sciences

Jing Zhang
Institute of Genetics and Developmental Biology, Chinese Academy of Sciences

Yanyan Li
Institute of Genetics and Developmental Biology

Yongpeng Li
Center for Agricultural Resources Research, Institute of Genetics and Developmental Biology

Yanxiao Niu
College of Life Sciences, Hebei Normal University

Wenli Zhang
Nanjing University https://orcid.org/0000-0003-0710-1966

Caixia Gao
Institute of Genetics and Developmental Biology https://orcid.org/0000-0003-3169-8248

Xiangdong Fu
State Key Laboratory of Plant Cell and Chromosome Engineering, Institute of Genetics and Developmental Biology, Chinese Academy of Sciences https://orcid.org/0000-0001-9285-7543

Yiping Tong

The State Key Laboratory for Plant Cell and Chromosome Engineering, Institute of Genetics and Developmental Biology, Chinese Academy of Sciences

Lei Wang

State Key Laboratory of Plant Genomics, Center for Agricultural Resources Research, Institute of Genetics and Developmental Biology, Chinese Academy of Sciences

HongQing Ling

Institute of Genetics and Developmental Biology, Chinese Academy of Sciences

Junming Li

Center for Agricultural Resources Research, Institute of Genetics and Developmental Biology, Chinese Academy of Sciences

---

Article

Keywords:

Posted Date: April 20th, 2023

DOI: https://doi.org/10.21203/rs.3.rs-2801336/v1

Additional Declarations: There is **NO** Competing Interest.

Version of Record: A version of this preprint was published at Nature Communications on December 12th, 2023. See the published version at https://doi.org/10.1038/s41467-023-44003-6.

Epigenetic modifications regulate cultivar-specific root development and metabolic adaptation to nitrogen availability in wheat

Hao Zhang[1,3], Zhiyuan Jin[4,5,6], Fa Cui[2], Long Zhao[1,3], Xiaoyu Zhang[1,3], Jinchao Chen[1,3], Jing Zhang[1,3], Yanyan Li[1,4], Yongpeng Li[4,5,6], Yanxiao Niu[5,6], Wenli Zhang[8], Caixia Gao[1,3], Xiangdong Fu[1,3], Yiping Tong[1,3], Lei Wang[1,4], Hong-Qing Ling[1,3,7*], Junming Li[4,5,6,*], Jun Xiao[1,3,6,9,*]

[1]State Key Laboratory of Plant Cell and Chromosome Engineering, Institute of Genetics and Developmental Biology, Chinese Academy of Sciences, Beijing 100101, China
[2]Key Laboratory of Molecular Module-Based Breeding of High Yield and Abiotic Resistant Plants in Universities of Shandong, College of Agriculture, Ludong University, Yantai 264025, China
[3]University of Chinese Academy of Sciences, Beijing 100049, China
[4]Center for Agricultural Resources Research, Institute of Genetics and Developmental Biology, Chinese Academy of Sciences, Shijiazhuang 050022, Hebei, China
[5]Ministry of Education Key Laboratory of Molecular and Cellular Biology, Hebei Research Center of the Basic Discipline of Cell Biology, Hebei Key Laboratory of Molecular and Cellular Biology, College of Life Sciences, Hebei Normal University, Shijiazhuang 050024, China
[6]Hebei Collaboration Innovation Center for Cell Signaling, Shijiazhuang, 050024, China
[7]Hainan Yazhou Bay Seed Laboratory, Sanya, Hainan, China.
[8]State Key Laboratory for Crop Genetics and Germplasm Enhancement and utilization, CICMCP, Nanjing Agricultural University, Nanjing, Jiangsu 210095, China
[9]Centre of Excellence for Plant and Microbial Science (CEPAMS), JIC-CAS, Beijing, China
[*]Correspondence to: hqling@genetics.ac.cn; ljm@sjziam.ac.cn; jxiao@genetics.ac.cn

Abstract

The breeding of crops with improved nitrogen use efficiency (NUE) is crucial for sustainable agriculture. Despite its importance, the way in which epigenetic modifications regulate cultivar-specific responses to low nitrogen (LN) constraints is not yet well understood. Here, we analyzed the chromatin landscapes in the roots, leaves, and seeds of two wheat cultivars (KN9204 and J411) that differ radically in NUE under varied nitrogen conditions. The chromatin regions responsible for regulating gene transcription exhibited clear cultivar-specificity between the two cultivars, and the regulation of nitrogen metabolism genes (NMGs) was closely linked to variation in histone modification levels instead of differences in DNA sequence. We also found that cultivar-specific histone modification regions contribute to the genetic regulation of NUE-related traits, such as the QTL locus of maximum root length of qMRL-7B. Additionally, LN-induced H3K27ac and H3K27me3 dynamics enhanced root growth more significantly in KN9204, while strengthened the nitrogen uptake system remarkably in J411. Evidence from histone deacetylase inhibitor treatment and transgenic plants with loss function of the H3K27me3 methyltransferase further showed that changes in epigenetic modifications can alter the strategy for root development and nitrogen uptake in response to LN constraint. Taken together, our data highlight the importance of epigenetic regulation in mediating cultivar-specific adaptation to LN in wheat.

Key words: epigenetic regulation; root architecture; nitrogen uptake; wheat; low nitrogen

Introduction

Improving nitrogen-use efficiency (NUE) has emerged as a pressing requirement for sustainable agriculture[1]. NUE is mainly composed of two components: N uptake efficiency (NUpE) and N utilize efficiency (NUtE). NUpE pertains to the acquisition of nitrogen from the soil, while NUtE signifies the yield generated per unit of nitrogen obtained. In situations where nitrogen availability is limited for crops such as winter wheat[2], barley[3], studies indicate that NUpE holds greater importance in determining NUE compared to NUtE. To enhance both NUE and grain yield, specifically under low nitrogen conditions, it is imperative to boost nitrogen uptake, which is predominantly regulated by nitrate transporters. The concentration of nitrate in soil can experience substantial fluctuations due to external environmental factors; as a result, root system architecture plays a vital role in the efficient absorption of nitrate. Numerous efforts have been undertaken to assist plants in acquiring adequate nitrogen under such conditions, such as overexpressing NRT2 (a high affinity nitrogen transporter)[4,5], and refining root architecture[6,7]. Nevertheless, further research is necessary to comprehensively understand the balance and coupling between root architecture response and nitrogen transporter expression, particularly when operating under low nitrogen conditions.

Kenong 9204 (KN9204) and Jing 411 (J411) are cultivars that exhibit diverse agricultural traits such as nitrogen use efficiency (NUE), root architecture, and productivity under low nitrogen conditions[2]. By utilizing these superior materials, we successfully identified several NUE-related quantitative trait loci (QTLs), encompassing factors such as root length, root tips, and grain protein content, derived from recombinant isogenic lines (RILs) generated through a cross between KN9204 and J411 in previous studies[8-10]. We recently completed the reference genome sequence of KN9204 and identified 882 nitrogen metabolism genes (NMGs)[11]. Comparative transcriptome analysis between KN9204 and J411 revealed different responsive programs under low nitrogen constraint, especially in the yield-related spike tissue and in seeds during reproductive development[11]. The underground tissues (roots) are not as well investigated. Past research emphasizes the importance of the root architecture system (RSA) for NUE[12] and the significant differences of RSA that exist between KN9204 and J411[2,8]. However, the regulatory mechanism underlying the diverse transcriptional programs linked to NUE in the roots of KN9204 and J411 still remains to be elucidated.

Recent studies have emphasized the crucial role that epigenetic factors play in regulating both nutrition uptake and metabolism, as well as the synergistic plant response to nutrient availability[13]. For example, the SET DOMAIN GROUP 8 (SDG8) gene is involved in regulating nitrogen (N) assimilation and lateral root response, by controlling the levels of H3K36me3 in response to changing nitrogen levels in *Arabidopsis*[14]. Similarly, the HISTONE DEACETYLASE 19 (HDA19) gene is responsible for controlling root cell elongation and modulating the expression of phosphorus (Pi)-homeostasis genes in *Arabidopsis* under phosphate starvation conditions[15]. In rice, the polycomb repressive complex 2 (PRC2), which is recruited by NITROGEN-MEDIATED TILLER GROWTH RESPONSE 5 (NGR5), regulates tillering by depositing H3K27me3 on branching-inhibitor genes[16]. Additionally, the H3K27me3 level at the AtNRT2.1 (nitrate transporter) locus influences root nitrate uptake, a process that is mediated by HIGH NITROGEN INSENSITIVE 9 (AtHNI9) and PRC2[17]. Despite these advances in understanding the role of epigenetics in nutrient uptake and metabolism of plants like Arabidopsis and rice, the co-regulation of these processes and their response to nutrient availability in wheat remains largely unexplored.

In this study, we used the CUT&Tag[18,19] to profile epigenomic modifications in two wheat cultivars, KN9204 and J411, for various histone modifications and histone variant in three different tissues

under varying nitrogen conditions. Our epigenomic maps offer a comprehensive understanding of the dynamic chromatin landscapes of these two wheat cultivars in response to low nitrogen conditions. By integrating our findings with previous QTL analysis, we also identified cultivar-specific transcription bias and epigenome divergence, particularly in the H3K27ac modification. Moreover, manipulating H3K27ac and H3K27me3 profiles through chemical inhibition or genetic mutation can significantly influence the LN adaptation strategy of different wheat cultivars.

Results

Profiling the tissue-specific chromatin landscape under different nitrogen conditions

To understand the epigenetic regulation of the transcriptomic dynamics (Fig. S1a), we did CUT&Tag of various histone modifications for the wheat cultivars KN9204 and J411 at normal nitrogen (NN) and LN conditions for roots (28 days), flag leaves (heading stage) and seeds (21 days after anthesis) (Fig. 1a), corresponding to transcriptomes generated previously[11]. The CUT&Tag assay showed reproducibility between two biological replicates for the various histone modifications (Fig.S1b). The majority of histone modification peaks were located in the distal region expected for H3K36me3 in wheat (Fig. S1c), as described in our recent report[19]. H3K27ac and H3K4me3 were associated with highly expressed genes, while H3K27me3 is enriched in low/non-expressed genes (Fig. S1d). H3K4me3 and H2A.Z did not show a preference for gene expression level (Fig. S1d). More than half of the H3K9me3 peaks were located in transposable elements (TEs) regions (Fig.S1e). Genes involved in biotic and abiotic stress responses had a higher H2A.Z level relative to that in developmental and hormone-related genes (Fig.S1f).

The chromatin state was systematically defined using ChromHMM[20], which integrated combinatorial patterns of various histone marks (Fig. 1b). Five major categories were formed from the fifteen chromatin states (CS) identified, including Promoter (CS1-4), Transcription (CS5-8), Enhancer-like (CS9-11), Repressive (CS12-14), and No signal (CS15), each with different genome coverage, TE enrichment, and gene expression level (Fig. 1b). Both the Promoter and Enhancer-like states were associated with H3K27ac, H3K4me3, and H3K27me3, but located in the transcription start site (TSS) and intergenic region, respectively (Fig. 1b). Repressive states were mainly enriched with H3K27me3, covering approximately 10% of the genome, while the no signal state accounted for a major portion (~83%) of the genome. Therefore, a limited portion of the genome (~7%) is transcribed or involved in transcriptional regulation in the context of various histone modifications (Fig. 1b).

We wonder how chromatin state dynamics reflect the differences between wheat cultivars, tissue types, and nitrogen conditions. For example, genes related to nitrate uptake in the root (*TaNRT2_3A*), assimilation in the leaf (*TaNIA_6D*), and amino acid storage in the seed (*TaPROT2_4D*) showed varied CS under LN condition in KN9204 (Fig. 1c). Generally, Enhancer-like CS was the most variable chromatin region between the different cultivars, while Promoter CS was primarily influenced by nitrogen availability (Fig. 1d). CS10 and CS9 showed the highest frequency of change between wheat cultivars, while CS10 and CS2 exhibited greater variability under different nitrogen availabilities (Fig. S1g). Furthermore, we calculated variability scores for different histone marks and found that H3K27ac and H3K27me3 exhibited

the highest variability scores among the different nitrogen conditions and between the wheat cultivars (Fig. 1e). Further examination of the distribution patterns (Fig. S1c) allowed us to categorize these histone marks into distal and promoter peaks and evaluate their variability using Pearson correlation analysis (Fig.1f, Fig.S1h). We observed that distal H3K27ac showed cultivar-specificity, while promoter H3K27ac showed greater tissue-specificity (Fig. 1f). For H3K27me3, both distal and promoter peaks exhibited cultivar-specificities (Fig. S1h). Therefore, distinct genomic regions with variable chromatin states are shaped by differences in wheat cultivars, tissue types, and nitrogen conditions, particularly with regards to H3K27ac and H3K27me3 marks.

Cultivar-bias expression of NMGs is mainly mediated by histone modification variations

NMGs are crucial for plants to uptake and utilize nitrogen, including genes that encode nitrate transporter (NPF, NRT2, NAR2, CLC, and SLAH), nitrate reductase (NIA, NIR), ammonium transporter (AMT), and amino acid transporter (APC) family members, as well as enzymes involved in ammonium assimilation (GS, GOGAT, GDH, ASN, AspAT) and transcription factors (TFs) related to N metabolism[21,22]. Previously, we have identified a total of 882 NMGs in wheat through sequence similarity comparisons to six other plant species including *Brachypodium distachyon,* barley, rice, sorghum, maize, and *Arabidopsis*[11].

We compared the NMGs between KN9204 and J411 for variations in DNA variation and H3K27ac modifications in promoter regions, and changes in transcriptional level. The results revealed that about 25% of NMGs displayed different levels of expression between KN9204 and J411 (FDR < 0.05, fold-change ≥ 1.5), while only around 5% of NMGs had DNA sequence variations in the promoter regulatory regions (Fig. 2a). The variation in expression of NMGs between KN9204 and J411 existed for different gene families in various tissues (Fig. 2b, Supplemental Table S1). For instance, in roots, the expression levels of *NRT2* and *NIA* in J411 were both higher under the LN condition relative to KN9204, while the *NPF* family genes was activated in KN9204 (Fig. S2a). Moreover, in flag leaves, *NIA* genes were up-regulated in KN9204, but not in J411. However, in seeds, the relative expression of genes that encode NPF and GS was much higher in KN9204 compared to J411 (Fig. S2a).

The bias expression of NMGs in different cultivars is unlikely to be affected by variations in the DNA sequence within their regulatory regions as only 16 genes overlapped (Fig. 2c, top). Rather, the majority of NMGs that showed cultivar-biased expression were marked by differential peaks of H3K27ac (66.9%) and H3K27me3 (45.6%) (Fig. 2c, Fig. S2b, Supplemental Table S1). In roots, the NRT2 family displayed similar changes in H3K27ac and H3K27me3 under LN/NN conditions in both cultivars but were more pronounced in J411 compared to KN9204 (Fig. 2d, top). For example, at the *TaNRT2_6A* (*TraesCS6A02G031000*) locus, H3K27ac gains and H3K27me3 losses in response to LN occurred in both cultivars but were more dramatic in J411 (Fig. 2e, top). This also aligns with the higher level of induced expression of *TaNRT2_6A* in J411 under LN conditions (Fig. 2e, top). TaNPF2.3, involved in nitrite transport from the root to the shoot[23], was activated in KN9204 with a decrease H3K27me3 under LN while it was accompanied by a significant decrease in H3K27ac in J411 (Fig. 2d, bottom). Consistently, *TaNPF2.3_7B* was increased in KN9204 but decreased in J411 under LN/NN conditions (Fig. 2e, bottom). Additionally, the nitrate contents in shoots relative

to roots were higher in KN9204 compared to J411 under LN conditions rather than NN conditions (Fig. 2f). Similarly, cultivar-specific H3K27ac dynamic in response to LN was associated with expression change of ammonium assimilation enzymes coding genes *GS* and *GOGAT* in seeds (Fig. S2c, d). Accordingly, KN9204 seeds have a higher protein content compared to J411 under LN conditions (Fig. S2e). Taken together, the varied levels of H3K27ac and H3K27me3 were associated with the expression bias of NMGs, leading to different nitrogen metabolism processes in KN9204 and J411.

Cultivar-specific H3K27ac influences NUE-related traits by transcriptional regulation

Given the importance of H3K27ac in regulating the chromatin state and expression patterns of NMGs across different tissues and cultivars at LN/NN, we extended to identify cultivar-specific H3K27ac regions using K-means clustering (Fig. 3a). In general, the cultivar-specific H3K27ac peaks were primarily over-represented in distal regions while under-represented in promoter and genic regions when compared to all H3K27ac peaks (Fig. 3b). Moreover, cultivar-specific H3K27ac-marked promoters had close associations with cultivar-specific expressed genes in roots, leaves, and seeds (Fig. 3c, Fig. S3a, b). For instance, H3K27ac-marked genes in KN9204 were associated with cell wall biogenesis and nutrient reservoir activity (e.g., *PROT1*, *LBD16*, *XTH19*, *CSLC5*) (Fig. 3c, Fig. S3c), while H3K27ac specifically modulated genes involved in flavonol biosynthesis in J411 (Fig. S3c).

The H3K27ac peaks in the distal region, specific to each cultivar, were found to be in the same location as H3K4me3 and H2A.Z (Fig. S3d), suggesting that these epigenetically modified hotspots serve as 'enhancers' in regulating gene expression[24-26]. A correlation between the H3K27ac and gene expression dynamics allowed us to assign these regions to potential targets within a 500 kb distance as reported previously[27,28] (Fig. S3e). A total of 58,493 unique pairs (22,003 distal H3K27ac regions and 6,357 target genes) between the distal cultivar-specific H3K27ac peaks and genes were identified (Fig. 3d), and the accuracy of the pairs was supported by a higher chromatin interaction ratio from published Hi-C data[29] (Fig. S3f). GO annotation of KN9204-specific distal H3K27ac-regulated genes showed enrichment in genes for cell wall synthesis, protoxylem development, and nutrient reservoir activity, which is similar to the KN9204-specific promoter H3K27ac-marked genes. Among them, several genes are known to be involved in nutrient transport to the shoot, such as *TaVND7*[30], *TaXTH25*[31]. No GO category was enriched in targets of J411-specific distal H3K27ac (Fig. 3d).

We examined the impact of cultivar-specific regulatory regions on DEGs located within QTLs identified via linkage analysis in a KN9204-J411 RIL population[8-10]. In comparison to DNA sequence variations within promoter regions, cultivar-specific distal H3K27ac regions exhibit a stronger correlation with DEGs located within QTL regions such as nitrogen uptake (Nup), nitrogen concentration (Nct), maximum root length (MRL), and grain protein content (GPC) (Fig. S3g). We noticed a significant enrichment of target genes of KN9204-specific H3K27ac peaks in QTLs that consisted of NUE related-traits, wherein the elite genetic loci originated from KN9204 (Fig. 3e, Supplemental Table S2). Whereas, the J411-specific H3K27ac region associated genes were enriched in QTLs linked to leaf size-related traits (Fig. 3e). For example, while examining the previously discovered qMRL-7B, we discovered 1,245 genes within the genetic region, of which 69 were DEGs, and only nine genes contained DNA sequence

variations within the promoter regions. In contrast, 34 genes had cultivar-specific distal H3K27ac peaks (Fig. 3f). We observed the higher expression levels of *TraesCS7B02G317800* (*TaHyPRP06_6B*) and *TraesCS7B02G326900* (*TaXTH25_7B*) in KN9204 compared to J411, which were correlated with KN9204-specific H3K27ac distal regulatory regions and were involved in regulating root development (Fig.3g, Fig. S3h). Furthermore, we confirmed the functional potential of these cultivar-specific regulatory regions through a luciferase reporter assay[32] (Fig.3h, Fig. S3i). Thus, both promoter and distal cultivar-specific H3K27ac regions play a significant role in transcriptional regulation and contain genetic variations that are responsible for NUE-related traits.

LN-induced H3K27ac dynamics affect divergent adaptive programs in KN9204 and J411

We further investigated the role of H3K27ac dynamics induced by LN in driving divergent adaptations between KN9204 and J411. H3K27ac shows varied dynamic patterns in different tissues under LN/NN conditions in KN9204 and J411 (Fig. 4a). KN9204 showed subtle changes in H3K27ac levels in roots, but more pronounced changes in flag leaves and seeds. Whereas J411 exhibited a significant loss and relatively lower gains in root but minor changes in above-ground tissues (Fig. 4a). Additionally, K-means clustering identified distinct H3K27ac dynamic patterns across different tissues in KN9204 and J411 (Fig. 4b, Fig. S4a).

Extensive loss of H3K27ac in roots of J411 (clusters C3, C5, and C6, n = 105,261) mainly located in distal regions (Fig. 4b, Fig. S4b). Whereas, gain of H3K27ac (clusters C4, C7, and C8, n = 49,527) were much less distributed in distal regions (Fig. 4b, Fig. S4b). Of note, many LN-induced H3K27ac-loss loci are specific to J411, but were maintained in KN9204 (C5 and C6 clusters). Such loss of H3K27ac in proximal regions (promoter and genic regions) caused down-regulation of genes that function in auxin homeostasis, cytokinin metabolism, and hormone signaling in J411 under LN/NN conditions (Fig. 4c). The gain of H3K27ac is linked to the activation of genes responsible for nitrate uptake, transport and assimilation, including *TaNRT2* and *TaNIA* (Fig. 4c). In contrast, gain-of-H3K27ac in roots of KN9204 activated genes involved in cytokinin biosynthesis, auxin polarity transport, transporters for carbohydrate and organic cations, such as *TaD27, TaPILS7,* and *TaLOG4* (Fig. 4c), which function in root growth under LN as reported[33,34]. Loss of H3K27ac in KN9204 led to down-regulation of genes involved in phosphate ion transport. Consistently, the root system of J411 has a lower response to LN as compared to KN9204, with more root tips and larger root diameters under LN conditions (Figs. 4d, e). This eventually translated into an increase in root surface area and a larger total root volume in KN9204. Thus, the dynamic changes in H3K27ac that occur in response to LN preferably enhanced root growth in KN9204 while they strengthened the nitrogen uptake system in root of J411. In KN9204 flag leaves, increased H3K27ac were found in genes related to sucrose metabolism and xylem development, while J411 had more of such genes related to reactive oxygen species response (Fig. S4c). In seeds, H3K27ac loss caused by LN occurred mainly in distal regions, thus have little influence on gene expression in both cultivars (Fig. S4d).

Whether the root morphological change in KN9204 and J411 under LN/NN is regulated by cultivar-biased LN-induced H3K27ac status? To determine this, we tested the effects of Trichostatin A (TSA), a chemical inhibitor of class I and II histone deacetylases (HDAC)[35], on

the H3K27ac pattern in wheat seedlings using a hydroponic culture system (See method for details). The effects of TSA treatment were validated by western blotting (Fig. S4e). Root growth was induced by LN in KN9204 in both the TSA-treated and the untreated group, as indicated by increased root tip numbers under LN compared to NN conditions (Fig. 4f). In J411 under the mock condition, root growth was not induced by LN as expected, but root tip numbers increased substantially by LN with TSA treatment (Fig. 4f). Therefore, TSA treatment inhibited the extensive LN-induced loss of H3K27ac in J411, which restored the root growth response of J411 to LN conditions.

H3K27me3 shapes distinct root developmental programs in KN9204 and J411 under LN

In addition to H3K27ac, H3K27me3 also showed varied dynamic patterns in roots, flag leaves, and seeds in response to LN in KN9204 and J411(Fig. 5a). In both KN9204 and J411, subtle changes in H3K27me3 occurred in flag leaves, while there were a large number of differential H3K27me3 regions in roots in J411 but in seeds in KN9204 (Fig. 5a). K-means clustering further identified different categories of dynamic H3K27me3 regions in roots and seeds under LN conditions for KN9204 and J411 (Fig. 5b, Fig. S5a).

The majority of the dynamic H3K27me3 regions were situated distally in both roots and seeds (Fig. S5b). In roots, the gain of H3K27me3 prevails compared to the loss in J411, for both proximal and distal regions (Fig. 5c), while for KN9204 there was more loss of H3K27me3 than gain in both regions, albeit with a smaller peak count than J411 (Fig. 5c). Additionally, genes marked with LN-induced gain-of-H3K27me3 (clusters C4, C5, and C7 in Fig. 5b) significantly overlapped with down-regulated genes in J411 (Fig. 5d, top). These genes are enriched in root growth-related processes, including auxin biosynthesis, regulation of cell differentiation, and root morphogenesis (Fig. 5e, top). For example, the gene for a *Mob1-like* transcription factor involved in root development[36] has increased H3K27me3 under LN conditions in J411 and the expression level is reduced, while no significant change in KN9204 (Fig. 5f, top). Conversely, the gain-of-H3K27me3 in KN9204 only overlapped with 24 genes that were down-regulated by LN (Fig. S5c), implying that LN-induced gain-of-H3K27me3 in roots might mainly reduce the root growth process in J411 but not so much in KN9204. Loss-of-H3K27me3 in KN9204 and J411 produced significant overlaps with genes where expression increased in response to LN (Fig. 5d, middle and bottom). Genes involved in the response to nitrite, nitrite transport, and nitrate assimilation were enriched in J411, while genes involved in nitrate transport and SL and GA biosynthetic processes, as well as primary cell wall biogenesis-related genes, were enriched in KN9204 (Fig. 5e, middle and bottom). For example, expression of *TaNAR2_4A* and *TaKAO2_4A* was activated separately in J411 and KN9204 with decreased H3K27me3 (Fig. 5f, middle and bottom). Thus, The LN-induced H3K27me3 loss in roots tends to activate root growth in KN9204. Conversely, in J411, the loss of H3K27me3 activates nitrite uptake and metabolism. In the seeds, gain or loss of H3K27me3 in KN9204 did not lead to much change in overall gene expression (Fig. S5d). The same is true for gain-of-H3K27me3 in J411 (Fig. S5d). However, loss-of-H3K27me3 induced a significant amount of up-regulation of gene expression in J411, though no specific GO term was enriched (Fig. S5d).

The deposition of H3K27me3 in plants depends on the recruitment of Polycomb repressive complex 2 (PRC2) by different DNA recognition factors[37,38]. To understand the drivers behind

the dynamic H3K27me3 landscape in two plant varieties (KN9204 and J411), we conducted a motif scanning analysis, which found that 'CGCCGCC' motif (50%) and 'GAGAGA' repeat (12.9%) were enriched in KN9204- and J411-specific dynamic H3K27me3 regions, respectively (Fig. 5g). Interestingly, these motifs were also present in Polycomb response element (PRE) fragments in *Arabidopsis*[37,39]. Based on transcription factor (TF)-DNA recognition in other species[40], TaERF9_5B/TaERF9_5D and TaBPC_4A were selected for interaction tests with PRC2 components. Using yeast two-hybrid (Y2H) and bimolecular fluorescence complementation (BiFC) assays, we verified that TaERF9_9B/TaERF9_5D (AP2/ERF family) and TaBPC_4A could interact with EMF2 and SWN (subunits of PRC2) *in vivo* (Fig. 5h, i). Notably, BPC had been reported to interact with SWN and influence root development in *Arabidopsis*[41]. Thus, different TFs likely mediate LN-induced divergent H3K27me3 changes between KN9204 and J411, resulting in different root development routes.

Rewiring H3K27me3 modulates root development and nitrate uptake in response to LN

We investigated whether H3K27me3 plays a critical role in root development under LN conditions. There are nine genes encode H3K27me3 methyltransferases within three triads (Fig. S6a), showing varied expressions in roots under different N conditions (Fig. S6b). Considering the high expression of *TaSWN* in roots (Fig. S6b), we used the CRISPR-Cas9 system to create knock-out mutants of *TaSWN* (*TraesCS4A02G121300*, *TraesCS4B02G181400*, and *TraesCS4D02G184600*) in the 'Bobwhite' (BW) background (Fig. S6c). Sequencing of transgenic wheat identified a *Taswn-cr* homozygous line with frameshift mutations in all three subgenome copies of *TaSWN* (Fig. S6c). We then used CUT&Tag to compare the genome-wide H3K27me3 patterns in the *Taswn-cr* and BW. The peak number and length of H3K27me3 in *Taswn-cr* was significantly decreased compared to BW (Fig. S6d). Similarly, the intensity of H3K27me3 on coding genes was decreased in *Taswn-cr* compared to BW (Fig. S6e). Therefore, TaSWN is indeed a H3K27me3 writer for some genomic areas in wheat.

Next, we profiled H3K27me3 patterns in BW and *Taswn-cr* to identify TaSWN-mediated H3K27me3 deposition in response to LN. K-means clustering identified different categories of dynamic H3K27me3 regions in BW and *Taswn-cr* under NN or LN conditions (Fig. 6a). Of note, the dynamic H3K27me3 peaks were predominantly located in distal regions, especially for clusters 1, 3, 6, and 7 (>80%) (Fig. S6f). Among them, clusters 1 and 6 showed reduced H3K27me3 in *Taswn-cr* compared to BW specifically under LN or both LN and NN conditions (Fig. 6a), which indicated a TaSWN-dependent manner. By overlapping with the LN-induced H3K27me3 peaks in KN9204 and J411 (Fig. 5b), we found that 10%-16% (n = 1,748, 14,094 separately) of the LN-induced H3K27me3 peaks in KN9204 or J411 were mediated by TaSWN (Fig. 6b). There were also more genes influenced by SWN in J411 (n = 959) compared to KN9204 (n = 86) (Fig. 6c, Fig. S6g), suggesting that H3K27me3 regulation has more weight in J411 than in KN9204. Furthermore, we identified a set of genes which gained H3K27me3 in J411 under LN/NN conditions but lost H3K27me3 in *Taswn-cr* compared to BW (Fig. 6d). This group of genes is involved in the root development process; examples are *MADS15*, *bHLH068*, and *MYB36* (Fig. 6d, e). The expression of these genes was induced in *Taswn-cr* under LN/NN, but no changes in BW (Fig. 6f). These results hint that TaSWN-mediated LN-induced gain-of-H3K27me3 in J411 partially reduces the root growth response to LN conditions. Therefore, we speculated that root growth in *Taswn-cr* plants would be more responsive to LN than BW.

Indeed, we found roots were more developed in *Taswn-cr* compared to BW under LN, as determined by total root length and the number of root tips (Fig. 6g, h). In addition, the relative level of induction of *NRT2* expression in response to LN in *Taswn-cr* was lower than BW (Fig. 6i, left), which were similar to KN9204 cultivar with more developed roots (Fig. 6i, right). Consistently, the nitrate uptake rate was higher in BW compared to *Taswn-cr* as measured by ^{15}N uptake assay under LN condition (Fig. 6j, left), which similar to the trend of J411 and KN9204 (Fig. 6j, right).

The comparison of root morphological changes, nitrate uptake rate and transcriptional profiles in response to LN between BW and Taswn-cr highlighted that H3K27me3 plays important role in balancing root growth and nitrogen metabolism under LN constraint. Rewiring H3K27me3 could influence wheat cultivars for the decision-making between significantly enhancing root growth or remarkably strengthening the nitrogen uptake system to adapt to low nitrogen environments.

Discussion

As the urgency to reduce nitrogen fertilizer application in crop production, considerable effort has been directed towards dissecting the genetic basis of NUE regulation in crops[42-44]. However, epigenetic regulation, which functions in coordinating with transcription factors to manipulate gene expression, is not well studied in wheat. To fill this gap, we generated epigenomic datasets for three different tissues in two wheat cultivars that differ with respect to NUE (KN9204 and J411) under different nitrogen conditions (Fig. 1). Our analysis revealed that the epigenome, which varies more than DNA sequence variation, plays an important role in mediating the cultivar-specific low nitrogen response.

Epigenetic variation contributes to cultivar-specific trait formation

Epigenetic modifications, especially H3K27me and H3K27ac, mediate transcriptional dynamics and contribute to different developmental programs or nitrogen metabolic processes between cultivars (Figs. 1, 2). Bias-expressed NMGs are associated with altered epigenetic regulation patterns rather than DNA sequence variations between KN9204 and J411 (Fig. 2). In addition, distal regulatory regions (H3K27ac and H3K27me3) clearly reflect cultivar specificity, with higher DNA sequence variations, and are associated with previously identified NUE-related QTLs (Fig. 3). In maize, many distal regulatory regions have been reported to regulate gene expression and are associated with agronomic trait variations[45,46]. Indeed, genes associated with cultivar-specific H3K27ac either in the promoter or in the distal region are enriched in QTL regions for mediating NUE-related agronomic traits, such as MRL, GPC, and Nup (Fig. 3), which could be good candidates for mediating the genetic difference between KN9204 and J411. Regarding the important role of epigenetic regulatory regions, more cultivars with defined NUE features could be used to profile the epigenome, especially H3K27ac and H3K27me3 in the future, which would enable Epi-GWAS analysis to uncover NUE regulatory mechanisms.

Epigenetic regulation balances root growth and nitrogen metabolism under LN constraint

To absorb adequate nitrogen in nitrogen-limiting conditions, cultivars with different NUE features have various strategies, such as triggering root growth to have more root tips and

increase the total root system volume in KN9204, or powering up the nitrate uptake machinery via up-regulation of NRT2 transporters in J411 (Fig. 1). Interestingly, the different adaptive strategies in roots between KN9204 and J411 are correlated with changes in the dynamic epigenome, especially for H3K27ac and H3K27me3 (Figs. 4, 5). Gain-of-H3K27ac and loss-of-H3K27me3 coordinately enhance the expression of root development-related genes in KN9204 under LN conditions, whereas loss-of-H3K27ac and gain-of-H3K27me3 reduce root development in J411 under LN, but rather activate nitrate uptake transporters via gain-of-H3K27ac and loss-of-H3K27me3 (Fig. 7). Several transcription factors show the potential to establish such epigenetic modification specificity via the recognition of certain cis-acting motifs and recruiting histone modification writers or erasers, such as ERFs and BPCs (Fig. 5). Thus, precise epigenetic modification modulates root development and nutrient absorption, which is likely to be a general mechanism for balancing plant growth and environmental stimulus response or adaptation[47]. However, it is presently unknown how such epigenetic modification behaves in a cultivar-specific manner. An interesting finding is that the potential histone writer or eraser-guiding TFs are located within the QTL regions linked to the MRL and Nup traits (Supplemental Table 3). Further analysis would elucidate how LN can trigger different response patterns in those TF genes in cultivars that vary with respect to NUE.

Manipulating epigenetic regulation to decouple root growth and nitrogen metabolism for NUE improvement in wheat

In addition to the correlation between cultivar-specific epigenetic dynamics and varied strategies in response to LN, we have shown that manipulating the epigenetic features could affect the strategy selection for LN adaptation. Chemical inhibition (TSA treatment) or genetic manipulation (*Taswn-cr*) that changes the epigenome landscape (H3K27ac and H3K27me3) could lead to altered root system development and coordinated *NRT2* induction intensity under LN constraint (Figs. 4, 6). Similarly, several reports have shown that adjusting histone modification contributes to the response and/or tolerance to stress, such as HDA6-regulated salt stress[48], and JMJ1-regulated dehydration stress[49]. Interestingly, the enhancement of root growth is likely coupled with the attenuated induction of the expression of nitrate transporter coding genes under LN constraint by histone modification, in particular H3K27me3 (Fig. 7). Theoretically speaking, precise epigenomic modification alterations at specific regions/genes could help to decouple such linkage, which could generate wheat with developed root architecture system and higher induction of nitrogen transporters simultaneously. To achieve this, instead of the genetic manipulation of the "writer" or "eraser" to histone modification, fine-tuning of the driver (for example ERFs) may serve as a better way of coordinating nitrogen metabolism and adaptive root growth to low nitrogen constraints in wheat cultivars.

Materials and methods

Plant materials and culture conditions

The root of KN9204 and J411 was harvested 4 weeks after transplanting in the nutrient solution, which corresponding to 28-day in previous study[11], and immediately frozen in liquid nitrogen and stored at -80°C. The nutrient solution for NN was as follows: 1 mM $Ca(NO_3)_2$, 0.2 mM KH_2PO_4, 0.5 mM $MgSO_4$, 1.5 mM KCl, 1.5 mM $CaCl_2$, 1×10^{-3} mM H_3BO_3, 5×10^{-5} mM $(NH_4)_6Mo_7O_{24}$, 5×10^{-4} mM $CuSO_4$, 1×10^{-3} mM $ZnSO_4$, 1×10^{-3} mM$MnSO_4$, 0.1 mM

Fe(III)–EDTA. For LN, 0.02mM $Ca(NO_3)_2$, 2.48 mM $CaCl_2$ (to compensate for the Ca^{2+} concentration in the nutrient solution), and other component was not changed. The flag leaf was harvested at heading stage[11] in the field (Shijiazhuang, China), and seed was also harvested 21DAA[11] in the field (shijiazhuang, China). In each NN plot, 300 kg/ha of diamine phosphate and 225 kg/ha of urea were applied before sowing, and 150 kg/ha of urea was applied at the elongation stage every year. In the LN plots, no N fertilizer (N-deficient) was applied during the growing period.

Generation of transgenic wheat plants

To obtain CRISPR transgenic wheat plants, the *pU6-gRNA* of *TaSWN* was annealed and inserted into *pJIT163-Ubi-Cas9* vector. All constructed vectors were transformed into callus to generate the transgenic plants.

To identify mutations in *TaSWN-4A*, *TaSWN-4B*, or *TaSWN-4D*, gene-specific primers were designed around the target site. Primers SWN-Check-F and SWN-Check-A-R were used to amplify *TaSWN-4A*, SWN-Check-F and SWN-Check-B-R were used to amplify *TaSWN-4B*, and SWN-Check-F and SWN-Check-D-R were used to amplify *TaSWN-4D*. Primer sequences were listed in Supplemental Table S4. PCR products were checked on agarose gels and genotyped by Sanger sequencing.

RNA-seq and CUT&Tag experiment

Total RNA was extracted using HiPure Plant RNA Mini Kit according to the manufacturer's instructions (Magen, R4111-02), and libraries were sequenced using an Illumina Novaseq platform.

CUT&Tag experiment were done follow the previous described method[19]. The nuclei were extracted by chooping fresh samples soaked in the HBM buffer (25 mM Tris-HCl pH 7.6, 0.44 M sucrose, 10 mM MgCl2, 0.1% Triton-X, 10 mM Beta-mercaptoethanol, 2 mM spermine, 1 mM PMSF, EDTA-free protease inhibitor cocktail). After overnight incubation with corresponding antibody in 4℃, the nuclei was incubated in 50μl wash buffer (20 mM HEPES pH 7.5; 150 mM NaCl; 0.5 mM Spermidine; 1× Protease inhibitor cocktail) with secondary antibody (1:100; Guinea Pig anti-Rabbit IgG antibody) at 4℃ for around 1-2 hour and then washed twice with wash buffer. pA-Tn5 complex (pA-Tn5 1:100 dilution in CT-300 buffer:20 mM HEPES pH 7.5; 300 mM NaCl; 0.5 mM Spermidine; 1× Protease inhibitor cocktail) was incubated with nuclei in 4℃ for 2-3h (Tn5, Vazyme, TD501-01). After washing twice with CT-300 buffer, the tagmentation of nuclei was done in 300 μl Tagmentation buffer (20 mM HEPES pH 7.5; 300 mM NaCl; 0.5 mM Spermidine; 1× Protease inhibitor cocktail; 10 mM MgCl2) in 37℃ for 1h. 10 μl 0.5M EDTA, 3 μl 10% SDS and 2.5 μl 20 mg/ml Protease K were added to stop tagmentation reaction. The DNA was extracted with phenol:chloroform:isoamyl alcohol, precipitated with ethanol, and resuspended in ddH2O. The library was amplified 17 cycles by Q5 high fidelity polymerase (NEB, M0491L). Antibodies used for histone modifications are the same as previous reported[19]. Libraries were purified with AMPure beads (Beckman, A63881) and sequenced using the Illumina Novaseq platform at Annoroad Gene Technology.

^{15}N-nitrate uptake activity assay

^{15}N-nitrate uptake activity assay was performed as described before[50]. Wheat seedlings were grown in LN nutrient solution (0.1 mM KNO_3) for 28 days, respectively. After that, the seedlings were subjected to a pre-treatment of 3 hours in LN nutrient solution (0.1 mM KNO_3). Subsequently, the seedings were transferred to LN (0.1 mM KNO_3 was replaced by 0.1 mM ^{15}N-KNO_3) nutrient solution for ^{15}N-labelling for a 3 hours. Post ^{15}N-labelling, the roots were washed using 0.1 mM $CaSO_4$ solution and deionized water. Finally, the shoots and roots of the seedlings were separately collected and dried at 70 °C until they reached a constant weight. Then, the samples were ground to fine powder and ^{15}N-content was detected using an isotope ratio mass spectrometer (Isoprime 100).

Nitrate (NO_3^-) content assay

Nitrate assay was performed as described before[51]. Standard curve was made based on different concentration of KNO_3 solution (deionized water as a control). Samples were boiled at 100 °C for 20 min. After Centrifuge of the boiled different samples, salicylic acid-sulphuric acid was added to supernatant. After incubation of 20 min, 8% (w/v) NaOH solution was added. After cool down of the samples, measure the OD_{410} value of each sample with the control for reference.

For samples collected of KN9204 and J411, grind each sample into powder in liquid nitrogen, detection procedure was done as described before. Finally, calculate the nitrate concentration using the following equation: Y = CV/W.

Y: nitrate content (μg/g),

C: nitrate concentration calculated with OD_{410} into standard curve (μg/ml),

V: the total volume of extracted sample (ml),

W: weight of sample (g).

Grain protein content assays

Grain protein content was measured by near-infrared reflectance spectroscopy (NIRS) with a Perten DA-7200 instrument (Perten Instruments, Huddinge, Sweden) and expressed on a 14 % moisture basis. The measurements were calibrated using calibration samples according to the manufacturer's instructions.

Luciferase reporter assay

The genomic sequence of distal regulatory region was amplified and fused in-frame with the *pMY155-mini35S* vector[32] to generate the reporter construct *cultivar-specific-regions-mini35Spro:LUC*. Primer sequences were listed in Supplemental Table S4. Then, *mini35Spro:LUC* (as control) and the reporter vector *cultivar-specific-regions* - *mini35Spro:LUC* were transformed into *A.tumefaciens* strain GV3101. The bacterial solution was injected to the back of the leaves of *Nicotiana benthamiana* (6-8 leaf stage) using a syringe with the needle removed. The *Nicotiana benthamiana* were cultivated for 2-3 days at a temperature of 22℃ and a light cycle of 16 h light/8 h dark. Firefly luciferase (LUC) and Renilla luciferase (REN) activities were measured using a dual luciferase assay reagent (Promega, VPE1910). And the relative intensity was calculated by ratio between relative ratio (LUC: REN) of cultivar-specific regions and empty vector.

Root system scanning

The root of different samples was scanned by ScanMaker i8000 plus, after analyzed by WinRHIZO software, five root traits were quantified, including total root length (Rl), root surface area (Rs), root volume (Rv), root diameter (Rd) and root tip number (Rt); and maximum root length is measured using a ruler.

LN response ratio (LRR) was calculated to reflect the root change under LN condition, which was (R_{LN}(root trait under LN condition) - R_{NN}(root trait under NN condition))/R_{NN}.

TSA treatment

TSA (V900931-5MG) was dissolved in DMSO, then directly add into nutrient solution (NN/LN) to final concentration of 2 μM, with DMSO as mock. After treatment of 4 days, the root was harvested and immediately frozen in liquid nitrogen and stored at -80°C.

Protein interaction test (Y2H and BiFC)

For the Y2H between PRC2 and TaERF9_5B/ TaERF9_5D/TaBPC_4A, Full-length of *TaERF9_5B*, *TaERF9_5D* and *TaBPC_4A* were amplified using specific primers (listed in Supplemental Table S4) and fused with GAL4 AD in the *pDEST22* vector. Full length of *TaEMF2-2A.2* and N-terminal of *TaSWN* were amplified using specific primers (listed in Supplemental Table S4) and fused with GAL4 BD in the *pDEST32* vector. Interactions in yeast were tested on the SD/-Trp/-Leu/-His/-Ade medium.

For the BiFC analysis, the cDNA of *TaERF9_5B/ TaERF9_5D/TaBPC_4A*and *TaEMF2-2A.2/TaSWN* was amplified with primers (listed in Supplemental Table S4) and cloned into *pSCYCE* and *pSCYNE* vectors containing either C- or N-terminal portions of the enhanced cyan fluorescent protein. The resulting constructs were transformed into *A. tumefaciens* strain GV3101. Then these strains were injected into tobacco leaves in different combinations with p19. The CFP fluorescence was observed with a confocal laser-scanning microscope (FluoView 1000, Olympus).

Western blot assays

Total histone proteins were extracted by using EpiQuik Total Histone Extraction Kit (OP-0006-100). The total histone proteins were then used for western blot using the antibodies listed below. Anti-H3 immunoblot was used as a loading control. Antibodies: anti-H3 (ab1791, Abcam), anti-H3K27ac (ab4729, Abcam). Immunoblotting was done by using the enhanced chemiluminescence (ECL) system.

RNA-seq Data Processing

Adapter sequence and low-quality reads of RNA-seq library was removed by fastp (0.20.1)[52], the cleaned reads was mapped to IWGSC Refseq v1.1 using hisat2 (2.1.0)[53], and gene expression was quantified by featureCount (2.0.1)[54]. Differentially expressed genes were evaluated using the DESeq2 package (1.34.0)[55] in R with an adjusted p value < 0.05 and log2 fold-change > 1. TPM (Transcripts Per Kilobase Million) values generated from the counts matrix were used to characterize gene expression and used for hierarchical clustering analysis.

For functional enrichment, GO annotation files were generated from IWGSC Annotation v1.1 and an R package clusterProfiler (4.2.2)[56] was used for enrichment analysis.

CUT&Tag Data Processing

Adapter sequence and low-quality reads of CUT&Tag library was removed by fastp (0.20.1)[52], the cleaned reads was mapped to IWGSC Refseq v1.1 using bwa mem algorithm (0.7.17)[57], We further filter the reads mapped with "samtools view -bS -F 1,804 -f 2 -q 30" to filter the low-quality mapped reads. Then the high-quality mapped reads were reduplicated using Picard-2.20.5-0. The de-duplicated bam files from two biological replicates were merged by samtools (1.5)[58], and merged bam file was converted into bigwig files using bamCoverage provided by deeptools (3.3.0) with parameters "-bs 10 --effectiveGenomeSize 14,600,000,000 --normalizeUsing RPKM --smoothLength 50". The bigwig files were visualized using deeptools (3.3.0)[59] and IGV (2.8.0.01)[60].

For peak calling, macs2 (2.1.4)[61] was used. For narrow peaks (H3K27ac, H3K4me3, and H2A.Z) and broad peaks (H3K27me3, H3K36me3, and H3K9me3), parameters "-p 1e-3 --keep-dup all -g 14600000000" and "--keep-dup all -g 14600000000 --broad --broad-cutoff 0.05" were used. Peak was annotated to the wheat genome using the R package ChIPseeker (v1.30.3)[62], as peaks annotated to three categories: promoter (-3000bp of TSS), genic (TSS to TES) and distal (other). The MAnorm package[63] was used for the quantitative comparison of CUT&Tag signals between samples with the following criteria: $|M \text{ value}| > 1$ and $P < 0.05$.

Chromatin state analysis

For chromatin state analysis, chromHMM (1.21)[20] was used. "BinarizeBam" and "LearnModel" commands with default parameters were used for chromatin-state (CS) annotation. Multiple models were trained on these data, with CS numbers ranging from 2 to 20. The 15-state model was selected because it captured all the key information of CS. In previous studies, 15-state models were similarly trained on rice[64] and *Arabidopsis*[65] data.

For chromatin states dynamic change analysis, bins (CS called, 200bp) were called dynamic if its state diverges between different samples. For variability score of histone modification, one minus jaccard index, which was calculated by bedtools (v2.29.2).

Distal regulatory region-gene assignment

The distal regulatory regions annotation strategy was largely based on a previous study[28]. Genes within 0.5M from a distal H3K27ac peak are considered candidate target genes. Then we generated null model as correlations between randomly selected peaks and randomly selected genes on different chromosomes, and enabling us to compute mean and standard deviation of this null distribution. For each potential link, after calculate correlation between gene expression (TPM) and distal H3K27ac signal (FPKM) in samples, we also compute p-values for the test correlations based on null model, then significantly pairs were selected as regulatory region-gene pairs.

Detection of transcription factor-binding motifs

To detect recruiter of dynamic H3K27me3 changes, we downloaded the position weightmatrices of plant motifs from the JASPAR database[40], the motifs was scanned by

FIMO(4.11.2) within dynamic H3K27me3 regions. And enrichment test of motifs detected were done by fisher test in R.

Statistical analysis

R (https://cran.r-project.org/;version 4.2.1) was used to compute statistics and generate plots if not specified. For two groups' comparison of data, the student's t-test was used, such as Fig.2f, Fig.3h, Fig.4d, Fig.4e, Fig.4f, Fig.6h, Fig.6j, Fig.S2e, Fig.S3i. For comparison of sequence data, Wilcox signed-rank test was used, such as Fig.2d, Fig.6f, Fig.S2c, Fig.S6d. For enrichment analysis, Fisher's exact test was used, such as Fig.2b, Fig.2c, Fig.3c, Fig.3d, Fig.3e, Fig.4c, Fig.5d, Fig.5e, Fig.5g, Fig.6c, Fig.6e, Fig.S3b, Fig.S3c, Fig.S4c, Fig.S4d, Fig.S5c, Fig.S5d, Fig.S6g.

Data availability

The raw sequence data were deposited in the Genome Sequence Archive (https://bigd.big.ac.cn/gsa) under accession number CRA009936; the transcriptome used was under BioProject accession numbers PRJCA004416; Hi-C data of wheat root was download from Gene Expression Omnibus (GEO) under accession number GSM3929164.

Code availability

Source code for analysis is available at https://github.com/ZhangHao-995/NUE-pipeline.

Acknowledgements

We thank Dr. Yijing Zhang from Fudan University for providing the *pMY155-mini35S* construct. This research was supported by National Key Research and Development Program of China (2021YFF1000401, 2021YFD1201500), National Natural Sciences Foundation of China (U22A6009), the Strategic Priority Research Program of the Chinese Academy of Sciences (XDA24010104), China Agriculture Research System of MOF and MARA (CARS-03), Hebei Natural Science Foundation (C2022503003) and China Agriculture Research System of MOF and MARA (CARS-03).

Author contributions

J.X. designed and supervised the research, J.X. H.Z. J.-M. L. H.-Q.L. wrote the manuscript. H.Z. performed CUT&Tag, RNA-seq, nitrate assay, TSA treatment, yeast two-hybrid assay and root scanning experiments; H.Z. and L.Z. performed data analysis. X.-Y.Z. performed plasmid construction, part of yeast two-hybrid assay, BiFC experiment, and luciferase reporter assay. F.C. performed determination of grain protein content. J.Z. performed Western blot; J.-C.C. performed plasmid construction for *Taswn-cr*. Z.-Y. J. and Y.-Y.L. performed ^{15}N-nitrate uptake activity assay. C.-X.G. provided *Taswn-cr* transgenic wheat. H.Z. and J.X. prepared all the figures. Y.-P.L., X.-Y.N., L.W., W.-L.Z., X.-D.F., and Y.-P.T. polished the manuscript. All authors discussed the results and commented on the manuscript.

Competing interests

The authors declare no competing interests.

Reference

1 Chen, X. *et al.* Producing more grain with lower environmental costs. *Nature* **514**, 486-489 (2014). https://doi.org:10.1038/nature13609

2 Wang, R. F. *et al.* Relationship between nitrogen uptake and use efficiency of winter wheat grown in the North China Plain. *Crop and Pasture Science* **62**, 504-514 (2011).

3 Anbessa, Y., Juskiw, P., Good, A., Nyachiro, J. & Helm, J. Genetic Variability in Nitrogen Use Efficiency of Spring Barley. *Crop Science* **49**, 1259-1269 (2009). https://doi.org:https://doi.org/10.2135/cropsci2008.09.0566

4 Chen, J. *et al.* Agronomic nitrogen-use efficiency of rice can be increased by driving OsNRT2.1 expression with the OsNAR2.1 promoter. *Plant Biotechnology Journal* **14**, 1705-1715 (2016). https://doi.org:https://doi.org/10.1111/pbi.12531

5 Fan, X. *et al.* Overexpression of a pH-sensitive nitrate transporter in rice increases crop yields. *Proceedings of the National Academy of Sciences* **113**, 7118-7123 (2016). https://doi.org:10.1073/pnas.1525184113

6 Gan, Y., Bernreiter, A., Filleur, S., Abram, B. & Forde, B. G. Overexpressing the ANR1 MADS-Box Gene in Transgenic Plants Provides New Insights into its Role in the Nitrate Regulation of Root Development. *Plant and Cell Physiology* **53**, 1003-1016 (2012). https://doi.org:10.1093/pcp/pcs050

7 Yu, L.-H. *et al.* MADS-Box Transcription Factor AGL21 Regulates Lateral Root Development and Responds to Multiple External and Physiological Signals. *Molecular Plant* **7**, 1653-1669 (2014). https://doi.org:10.1093/mp/ssu088

8 Fan, X. *et al.* Identification of QTL regions for seedling root traits and their effect on nitrogen use efficiency in wheat (Triticum aestivum L.). *Theoretical and Applied Genetics* **131**, 2677-2698 (2018). https://doi.org:10.1007/s00122-018-3183-6

9 Cui, F. *et al.* QTL detection for wheat kernel size and quality and the responses of these traits to low nitrogen stress. *Theoretical and Applied Genetics* **129**, 469-484 (2016). https://doi.org:10.1007/s00122-015-2641-7

10 Zhao, C. *et al.* QTL for flag leaf size and their influence on yield-related traits in wheat. *Euphytica* **214**, 209 (2018). https://doi.org:10.1007/s10681-018-2288-y

11 Shi, X. *et al.* Comparative genomic and transcriptomic analyses uncover the molecular basis of high nitrogen-use efficiency in the wheat cultivar Kenong 9204. *Molecular Plant* **15**, 1440-1456 (2022). https://doi.org:10.1016/j.molp.2022.07.008

12 Garnett, T., Conn, V. & Kaiser, B. N. Root based approaches to improving nitrogen use efficiency in plants. *Plant Cell Environ* **32**, 1272-1283 (2009). https://doi.org:10.1111/j.1365-3040.2009.02011.x

13 Sere, D. & Martin, A. Epigenetic regulation: another layer in plant nutrition. *Plant Signal Behav* **15**, 1686236 (2020). https://doi.org:10.1080/15592324.2019.1686236

14 Li, Y. *et al.* SDG8-Mediated Histone Methylation and RNA Processing Function in the Response to Nitrate Signaling. *Plant Physiol* **182**, 215-227 (2020). https://doi.org:10.1104/pp.19.00682

15 Chen, C. Y., Wu, K. & Schmidt, W. The histone deacetylase HDA19 controls root cell elongation and modulates a subset of phosphate starvation responses in Arabidopsis. *Sci Rep* **5**, 15708 (2015). https://doi.org:10.1038/srep15708

16 Wu, K. *et al.* Enhanced sustainable green revolution yield via nitrogen-responsive chromatin modulation in rice. *Science* **367** (2020). https://doi.org:10.1126/science.aaz2046

17 Widiez, T. *et al.* High nitrogen insensitive 9 (HNI9)-mediated systemic repression of root NO3- uptake is associated with changes in histone methylation. *Proc Natl Acad Sci U S A* **108**, 13329-13334 (2011). https://doi.org:10.1073/pnas.1017863108

18 Kaya-Okur, H. S. *et al.* CUT&Tag for efficient epigenomic profiling of small samples and

single cells. *Nat Commun* **10**, 1930 (2019). https://doi.org:10.1038/s41467-019-09982-5

19 Zhao, L. *et al.* Dynamic chromatin regulatory programs during embryogenesis of hexaploid wheat. *Genome Biology* **24**, 7 (2023). https://doi.org:10.1186/s13059-022-02844-2

20 Ernst, J. & Kellis, M. Chromatin-state discovery and genome annotation with ChromHMM. *Nat Protoc* **12**, 2478-2492 (2017). https://doi.org:10.1038/nprot.2017.124

21 Wang, Y. Y., Cheng, Y. H., Chen, K. E. & Tsay, Y. F. Nitrate Transport, Signaling, and Use Efficiency. *Annu Rev Plant Biol* **69**, 85-122 (2018). https://doi.org:10.1146/annurev-arplant-042817-040056

22 Krapp, A. Plant nitrogen assimilation and its regulation: a complex puzzle with missing pieces. *Curr Opin Plant Biol* **25**, 115-122 (2015). https://doi.org:10.1016/j.pbi.2015.05.010

23 Taochy, C. *et al.* The Arabidopsis root stele transporter NPF2.3 contributes to nitrate translocation to shoots under salt stress. *Plant J* **83**, 466-479 (2015). https://doi.org:10.1111/tpj.12901

24 Giaimo, B. D., Ferrante, F., Herchenrother, A., Hake, S. B. & Borggrefe, T. The histone variant H2A.Z in gene regulation. *Epigenetics Chromatin* **12**, 37 (2019). https://doi.org:10.1186/s13072-019-0274-9

25 Russ, B. E. *et al.* Regulation of H3K4me3 at Transcriptional Enhancers Characterizes Acquisition of Virus-Specific CD8(+) T Cell-Lineage-Specific Function. *Cell Rep* **21**, 3624-3636 (2017). https://doi.org:10.1016/j.celrep.2017.11.097

26 Calo, E. & Wysocka, J. Modification of enhancer chromatin: what, how, and why? *Mol Cell* **49**, 825-837 (2013). https://doi.org:10.1016/j.molcel.2013.01.038

27 Wang, M. *et al.* An atlas of wheat epigenetic regulatory elements reveals subgenome divergence in the regulation of development and stress responses. *Plant Cell* **33**, 865-881 (2021). https://doi.org:10.1093/plcell/koab028

28 Trevino, A. E. *et al.* Chromatin accessibility dynamics in a model of human forebrain development. *Science* **367** (2020). https://doi.org:10.1126/science.aay1645

29 Concia, L. *et al.* Wheat chromatin architecture is organized in genome territories and transcription factories. *Genome Biol* **21**, 104 (2020). https://doi.org:10.1186/s13059-020-01998-1

30 Yamaguchi, M. *et al.* VASCULAR-RELATED NAC-DOMAIN7 directly regulates the expression of a broad range of genes for xylem vessel formation. *Plant J* **66**, 579-590 (2011). https://doi.org:10.1111/j.1365-313X.2011.04514.x

31 Sasidharan, R. *et al.* Light quality-mediated petiole elongation in Arabidopsis during shade avoidance involves cell wall modification by xyloglucan endotransglucosylase/hydrolases. *Plant Physiol* **154**, 978-990 (2010). https://doi.org:10.1104/pp.110.162057

32 Li, Z. *et al.* The bread wheat epigenomic map reveals distinct chromatin architectural and evolutionary features of functional genetic elements. *Genome Biol* **20**, 139 (2019). https://doi.org:10.1186/s13059-019-1746-8

33 Tokunaga, H. *et al.* Arabidopsis lonely guy (LOG) multiple mutants reveal a central role of the LOG-dependent pathway in cytokinin activation. *Plant J* **69**, 355-365 (2012). https://doi.org:10.1111/j.1365-313X.2011.04795.x

34 Barbez, E. *et al.* A novel putative auxin carrier family regulates intracellular auxin homeostasis in plants. *Nature* **485**, 119-122 (2012). https://doi.org:10.1038/nature11001

35 Yoshida, M., Kijima, M., Akita, M. & Beppu, T. Potent and specific inhibition of mammalian histone deacetylase both in vivo and in vitro by trichostatin A. *Journal of Biological Chemistry* **265**, 17174-17179 (1990). https://doi.org:10.1016/s0021-9258(17)44885-x

36 Gonin, M. *et al.* CROWN ROOTLESS1 binds DNA with a relaxed specificity and activates OsROP and OsbHLH044 genes involved in crown root formation in rice. *Plant J* **111**, 546-566 (2022). https://doi.org:10.1111/tpj.15838

37 Xiao, J. *et al.* Cis and trans determinants of epigenetic silencing by Polycomb repressive complex 2 in Arabidopsis. *Nat Genet* **49**, 1546-1552 (2017). https://doi.org:10.1038/ng.3937

38 Bieluszewski, T., Xiao, J., Yang, Y. & Wagner, D. PRC2 activity, recruitment, and silencing: a comparative perspective. *Trends in Plant Science* **26**, 1186-1198 (2021). https://doi.org:10.1016/j.tplants.2021.06.006

39 Zhou, Y. *et al.* Telobox motifs recruit CLF/SWN–PRC2 for H3K27me3 deposition via TRB factors in Arabidopsis. *Nature Genetics* **50**, 638-644 (2018). https://doi.org:10.1038/s41588-018-0109-9

40 Fornes, O. *et al.* JASPAR 2020: update of the open-access database of transcription factor binding profiles. *Nucleic Acids Res* **48**, D87-D92 (2020). https://doi.org:10.1093/nar/gkz1001

41 Mu, Y. *et al.* BASIC PENTACYSTEINE Proteins Repress ABSCISIC ACID INSENSITIVE4 Expression via Direct Recruitment of the Polycomb-Repressive Complex 2 in Arabidopsis Root Development. *Plant Cell Physiol* **58**, 607-621 (2017). https://doi.org:10.1093/pcp/pcx006

42 Li, H., Hu, B. & Chu, C. Nitrogen use efficiency in crops: lessons from Arabidopsis and rice. *J Exp Bot* **68**, 2477-2488 (2017). https://doi.org:10.1093/jxb/erx101

43 Swarbreck, S. M. *et al.* A Roadmap for Lowering Crop Nitrogen Requirement. *Trends Plant Sci* **24**, 892-904 (2019). https://doi.org:10.1016/j.tplants.2019.06.006

44 Han, M., Okamoto, M., Beatty, P. H., Rothstein, S. J. & Good, A. G. The Genetics of Nitrogen Use Efficiency in Crop Plants. *Annu Rev Genet* **49**, 269-289 (2015). https://doi.org:10.1146/annurev-genet-112414-055037

45 Ricci, W. A. *et al.* Widespread long-range cis-regulatory elements in the maize genome. *Nat Plants* **5**, 1237-1249 (2019). https://doi.org:10.1038/s41477-019-0547-0

46 Li, E. *et al.* Long-range interactions between proximal and distal regulatory regions in maize. *Nat Commun* **10**, 2633 (2019). https://doi.org:10.1038/s41467-019-10603-4

47 Xiao, J. *et al.* Wheat genomic study for genetic improvement of traits in China. *Sci China Life Sci* **65**, 1718-1775 (2022). https://doi.org:10.1007/s11427-022-2178-7

48 Luo, M. *et al.* HD2C interacts with HDA6 and is involved in ABA and salt stress response in Arabidopsis. *J Exp Bot* **63**, 3297-3306 (2012). https://doi.org:10.1093/jxb/ers059

49 Huang, S. *et al.* Arabidopsis histone H3K4 demethylase JMJ17 functions in dehydration stress response. *New Phytol* **223**, 1372-1387 (2019). https://doi.org:10.1111/nph.15874

50 Liu, Y., Hu, B. & Chu, C. 15N-nitrate Uptake Activity and Root-to-shoot Transport Assay in Rice. *Bio-Protocol* **6** (2016). https://doi.org:10.21769/BioProtoc.1897

51 Zhao, L. & Wang, Y. Nitrate Assay for Plant Tissues. *Bio Protoc* **7**, e2029 (2017). https://doi.org:10.21769/BioProtoc.2029

52 Chen, S., Zhou, Y., Chen, Y. & Gu, J. fastp: an ultra-fast all-in-one FASTQ preprocessor. *Bioinformatics* **34**, i884-i890 (2018). https://doi.org:10.1093/bioinformatics/bty560

53 Kim, D., Paggi, J. M., Park, C., Bennett, C. & Salzberg, S. L. Graph-based genome alignment and genotyping with HISAT2 and HISAT-genotype. *Nat Biotechnol* **37**, 907-915 (2019). https://doi.org:10.1038/s41587-019-0201-4

54 Liao, Y., Smyth, G. K. & Shi, W. featureCounts: an efficient general purpose program for assigning sequence reads to genomic features. *Bioinformatics* **30**, 923-930 (2014). https://doi.org:10.1093/bioinformatics/btt656

55 Love, M. I., Huber, W. & Anders, S. Moderated estimation of fold change and dispersion for RNA-seq data with DESeq2. *Genome Biol* **15**, 550 (2014). https://doi.org:10.1186/s13059-014-0550-8

56 Wu, T. *et al.* clusterProfiler 4.0: A universal enrichment tool for interpreting omics data. *Innovation (Camb)* **2**, 100141 (2021). https://doi.org:10.1016/j.xinn.2021.100141

57 Li, H. Aligning sequence reads, clone sequences and assembly contigs with BWA-MEM.

arXiv (2013). https://doi.org:10.48550/arXiv.1303.3997
58 Danecek, P. *et al.* Twelve years of SAMtools and BCFtools. *GigaScience* **10**, giab008 (2021). https://doi.org:10.1093/gigascience/giab008
59 Ramirez, F. *et al.* deepTools2: a next generation web server for deep-sequencing data analysis. *Nucleic Acids Res* **44**, W160-165 (2016). https://doi.org:10.1093/nar/gkw257
60 Robinson, J. T. *et al.* Integrative genomics viewer. *Nature Biotechnology* **29**, 24-26 (2011). https://doi.org:10.1038/nbt.1754
61 Zhang, Y. *et al.* Model-based Analysis of ChIP-Seq (MACS). *Genome Biology* **9**, R137 (2008). https://doi.org:10.1186/gb-2008-9-9-r137
62 Yu, G., Wang, L.-G. & He, Q.-Y. ChIPseeker: an R/Bioconductor package for ChIP peak annotation, comparison and visualization. *Bioinformatics* **31**, 2382-2383 (2015). https://doi.org:10.1093/bioinformatics/btv145
63 Shao, Z., Zhang, Y., Yuan, G.-C., Orkin, S. H. & Waxman, D. J. MAnorm: a robust model for quantitative comparison of ChIP-Seq data sets. *Genome Biology* **13**, R16 (2012). https://doi.org:10.1186/gb-2012-13-3-r16
64 Zhao, L. *et al.* Integrative analysis of reference epigenomes in 20 rice varieties. *Nat Commun* **11**, 2658 (2020). https://doi.org:10.1038/s41467-020-16457-5
65 Wu, L. Y. *et al.* Dynamic chromatin state profiling reveals regulatory roles of auxin and cytokinin in shoot regeneration. *Dev Cell* **57**, 526-542 e527 (2022). https://doi.org:10.1016/j.devcel.2021.12.019

Figure legends

Fig. 1. A 15-state model characterizes the dynamic chromatin landscape in KN9204 and J411

a. Experimental design for generating the epigenomic data sets in KN9204 and J411 under different nitrogen conditions.
b. Chromatin state definitions, genomic annotation enrichments, and expression levels of genes associated with each chromatin state. Chromatin states could be mainly organized into five categories: Pr (promoter), Tr (transcription), En (enhancer-like), Re (repressive), and Ns (No signal) states.
c. Schematic diagrams representing the chromatin state dynamics under different nitrogen conditions and tissues. State colors are as in (b).
d. The fractions of bases for the states of the five categories that vary between cultivar difference and nitrogen availability.
e. Variability scores of histone modifications between cultivar difference and nitrogen availability.
f. Cross-correlation heatmaps of all H3K27ac peaks which were located in the distal or promoter regions separately for the two cultivars and the two nitrogen conditions. Abbreviations were as follow: KN_NN_R: KN9204_NN_Root, KN_NN_L: KN9204_NN_Leaf, KN_NN_S: KN9204_NN_Seed, KN_LN_R: KN9204_LN_Root, KN_LN_L: KN9204_LN_Leaf, KN_LN_S: KN9204_LN_Seed, J4_NN_R: J411_NN_Root, J4_NN_L: J411_NN_Leaf, J4_NN_S: J411_NN_Seed, J4_LN_R:

J411_LN_Root, J4_LN_L: J411_LN_Leaf, J4_LN_S: J411_LN_Seed.

Fig. 2. Epigenomic variations are vital to the expression bias of NMGs

a. Fraction of the regulatory regions and expression variation of nitrogen metabolism genes (NMGs) between wheat cultivars KN9204 and J411. Abbreviations were as follow: NPF: NRT1/PTR FAMILY, NRT2: Nitrate transporter 2, CLC: Chloride channel protein, SLAH: Slow anion channel-associated homologues, AMT: Ammonium transporter, APC: The amino acid–polyamine–choline transporter superfamily, NIA: Nitrate reductase, NIR: Nitrite reductase, GS: Glutamine synthetase, GOGAT: Glutamate synthase, ASN: Asparagine synthetase, AspAT: Aspartate aminotransferase, GDH: Glutamate dehydrogenase, TF: transcription factor.
b. Enrichment of LN-induced differentially-expressed NMGs based on their functional category in three tissues (Fisher's exact test was used to calculate the *p*-values for the overlaps). Abbreviations were same with (a).
c. Proportion of NMGs showing expression variation between KN9204 and J411 with regulatory region variation (top panel), H3K27ac variation (middle panel), and H3K27me3 variation (bottom panel).
d. Histone modification (H3K27ac and H3K27me3) levels of NRT2 and NPF2.3 in the roots of KN9204 and J411 between the two nitrogen availability levels (Wilcox test: ns: $p > 0.05$; *: $p \leq 0.05$; **: $p \leq 0.01$; ****: $p \leq 0.0001$).
e. Representative tracks showing histone modifications and transcriptional changes of *TaNRT2_6B* and *TaNPF2.3_7B* in roots for the two wheat cultivars and two nitrogen levels.
f. Nitrate content of shoots and roots of KN9204 and J411 under two nitrogen conditions (Student's *t*-test; ns: $p > 0.05$; *: $p \leq 0.05$).

Fig. 3. Distal regulatory region divergence is involved in NUE-trait variation between KN9204 and J411

a. K-means clustering of the variable H3K27ac peaks.
b. Peak distribution (distal, genic, or promoter) of cultivar-specific H3K27ac peaks in the wheat genome.
c. Mean gene expression in J411 (x-axis) versus mean gene expression in KN9204 (y-axis) for genes associated with proximal cultivar-biased H3K27ac peaks separately in the roots (top panel). Overlap between genes marked by cultivar-specific H3K27ac and DEGs between cultivars (blue circle) (bottom panel) (Fisher's exact test was used to calculate the *p*-values for the overlaps).
d. Assignment of distal cultivar-specific H3K27ac peaks to potential targets; representative genes and GO enrichment are shown on the right, and representative case is shown at the bottom. Abbreviations were as follow: NN_R: NN_Root, NN_L: NN_Leaf, NN_S: NN_Seed, LN_R: LN_Root, LN_L: LN_Leaf, LN_S: LN_Seed.
e. Enrichment of target genes with distal cultivar-specific H3K27ac peaks in QTLs between KN9204 and J411 (Fisher's exact test was used to calculate the *p*-values for the enrichment). Abbreviation: Rt: root tip number; Rd: root diameter; Nup: Nitrogen uptake content; Nct: Nitrogen concentration; MRL: Maximum root length; TKW: Thousand-kernel weight; GPC: Grain protein content; Rs: Root surface area; Rdw: Root dry weight; Ls: flag leaf size.
f. Schematic diagram illustrating the process used to narrow down potential key genes

regulated by distal cultivar-specific regulation in the QTL regions (*QMRL-7B* in this case).

g. Representative tracks of *TaHyPRP06* regulated by distal cultivar-specific H3K27ac peaks in *QMRL-7B*. Abbreviations were as follow: NN_R: NN_Root, LN_R: LN_Root.

h. Luciferase reporter assay of cultivar-specific H3K27ac regions in track shown in (g) and Fig.S3.h (Student's *t*-test; ns: $p > 0.05$; *: $p \leq 0.05$).

Fig. 4. Dynamics of H3K27ac reveals the divergent strategies of KN9204 and J411 to low nitrogen conditions

a. The number of differential H3K27ac peaks in response to LN of three tissues (seeds, roots, leaves) in KN9204 and J411.

b. Heatmaps showing the differential H3K27ac peaks in eight clusters in the roots of KN9204 and J411 under NN and LN conditions.

c. Dynamic proximal H3K27ac peaks and corresponding gene expression changes in the roots of KN9204 and J411. Representative genes and GO (gene ontology) enrichments are shown on the right. Abbreviations were as follow: KN_NN_R: KN9204_NN_Root, KN_LN_R: KN9204_LN_Root, J4_NN_R: J411_NN_Root, J4_LN_R: J411_LN_Root.

d. The LN-response-ratio (LRR) of root systems for KN9204 and J411 (Student's *t*-test; ns: $p > 0.05$; *: $p \leq 0.05$).

e. The number of root tips in KN9204 and J411 plants under different nitrogen conditions (Student's *t*-test; ns: $p > 0.05$; *: $p \leq 0.05$).

f. Phenotypes of the root systems of KN9204 and J411 seedlings in the control (mock) and TSA treatments (2 μM) under different nitrogen conditions. Scale bars=5cm. The right panel is the LRR of the root tips (Student's *t*-test; ns: $p > 0.05$; *: $p \leq 0.05$).

Fig. 5. Different trends in H3K27me3 shapes adaptation bias between the cultivars KN9204 and J411

a. The number of differential (gain or loss) H3K27me3 peaks in response to LN of three tissues in KN9204 and J411.

b. Heatmaps showing the differential H3K27me3 peaks in the seven clusters in the roots of KN9204 and J411 under LN and NN conditions.

c. The number of differential H3K27me3 peaks (in proximal or distal regions) in the root of KN9204 and J411 plants in response to LN.

d. Overlap between genes with dynamic changes in H3K27me3 and DEGs in the roots (Fisher's exact test was used to calculate the *p*-values for the overlaps).

e. GO enrichment of the overlapping genes related to (d).

f. Representative tracks showing H3K27me3 and transcriptional changes in *TaMob1L_6D* (top panel), *TaNAR2_4A* (middle panel), and *TaKAO2_4A* (bottom panel) for the two cultivars under LN and NN. Abbreviations were as follow: KN_NN_R: KN9204_NN_Root, KN_LN_R: KN9204_LN_Root, J4_NN_R: J411_NN_Root, J4_LN_R: J411_LN_Root.

g. Sequence motif enrichment for the up-regulated H3K27me3 peaks under LN conditions in KN9204 and J411 (Fisher's exact test was used to calculate the *p*-values for the enrichment).

h. Yeast two-hybrid (Y2H) assays showing the interaction between TaERF9_5B/TaERF9_5D/TaBPC_4A and TaEMF2-2A.2/TaSWN (components of PRC2).

Transformed yeast cells were grown on synthetic media lacking Leu and Trp (-WL) and Leu, Trp, His, and Ade (-WLHA) or Leu, Trp, and His (-WLH) with 1mM 3AT.

i. BiFC analysis of the interaction between TaERF9_5B/TaERF9_5D/TaBPC_4A and TaSWN-N/TaEMF2_2A.2. Scale bars = 10 mm.

Fig. 6. Rewiring H3K27me3 strengthens root adaptation to low nitrogen fertilization level

a. Heatmaps showing the differential H3K27me3 peaks in 'BobWhite' (BW) and the *Taswn-cr* mutant plants in the eight clusters under NN and LN conditions.
b. The proportion of TaSWN-dependent peaks in the up-regulated H3K27me3 peaks under LN conditions in KN9204 and J411.
c. Overlap between genes marked by TaSWN-dependent H3K27me3 and marked by gain-of-H3K27me3 under LN conditions in J411 (Fisher's exact test was used to calculate the *p*-values for the overlap).
d. Dynamic changes in the TaSWN-dependent H3K27me3 peaks under different nitrogen conditions (NN and LN) in KN9204, J411, BW, and *Taswn-cr* plants. Representative gene names are shown on the right.
e. GO enrichment of the overlapping genes related to (d).
f. The expression changes and fold-changes of the genes in (d). (Wilcoxon test: ns: $p > 0.05$; ****: $p \leq 0.0001$) FC: fold-change.
g. Scans of root systems of BW and *Taswn-cr* seedlings grown under different nitrogen conditions. Scale bars = 5 cm.
h. The number of root tips and total length of the root systems for BW and *Taswn-cr* seedlings grown under different nitrogen conditions. (Student's *t*-test; ns: $p > 0.05$; *: $p \leq 0.05$).
i. The fold-changes in the expression of *NRT2* genes in BW, *Taswn-cr*, J411, and KN9204 seedlings grown under different nitrogen conditions.
j. ^{15}N-nitrate uptake activity of different seedlings (KN9204, J411, BW, and *Taswn-cr*) grown under LN conditions (Student's *t*-test; ns: $p > 0.05$; *: $p \leq 0.05$).

Fig. 7. The balanced model of epigenetic regulation for divergent strategies to LN conditions in wheat

In the low-nitrogen condition (Input, left), different adaptation strategy of wheat is selected from the balance between root system development and nitrate uptake transporters (NRT2s). great gain-of-H3K27ac enhance the expression of root development-related genes in KN9204, Conversely, greater gain-of-H3K27me3 and minor gain-of-H3K27ac reduce root development in J411, but with an associated increase in nitrate uptake transporters (NRT2s) via gain-of-H3K27ac. After the knock-out of TaSWN (*Taswn-cr*), there is de-repression of root development, accompanied by the loss of H3K27me3 (Decision making, middle). Phenotypically, KN9204 has a developed root architecture (higher expression of root development genes) but lower nitrate uptake rate per unit weight (lower expression of NRT2s). In contrast, J411 has a diverse selection with regards to this balance (Output, right).

Fig. S1. NUE epigenome dataset

a. The number of DEGs in the tissues in response to LN in KN9204 and J411.
b. PCA plots of H3K27ac, H3K27me3, H3K4me3, H3K9me3, H3K36me3, and H2A.Z in the NUE epigenome dataset. Each dot represents one sample. Two biological replicates were

sequenced for each stage. Abbreviations were as follow: KN_NN_R_1: KN9204_NN_Root rep1, KN_NN_R_2: KN9204_NN_Root rep2, KN_NN_L_1: KN9204_NN_Leaf rep1, KN_NN_L_2: KN9204_NN_Leaf rep2, KN_NN_S_1: KN9204_NN_Seed rep1, KN_NN_S_2: KN9204_NN_Seed rep2, KN_LN_R_1: KN9204_LN_Root rep1, KN_LN_R_2: KN9204_LN_Root rep2, KN_LN_L_1: KN9204_LN_Leaf rep1, KN_LN_L_2: KN9204_LN_Leaf rep2, KN_LN_S_1: KN9204_LN_Seed rep1, KN_LN_S_2: KN9204_LN_Seed rep2, J4_NN_R_1: J411_NN_Root rep1, J4_NN_R_2: J411_NN_Root rep2, J4_NN_L_1: J411_NN_Leaf rep1, J4_NN_L_2: J411_NN_Leaf rep2, J4_NN_S_1: J411_NN_Seed rep1, J4_NN_S_2: J411_NN_Seed rep2, J4_LN_R_1: J411_LN_Root rep1, J4_LN_R_2: J411_LN_Root rep2, J4_LN_L_1: J411_LN_Leaf rep1, J4_LN_L_2: J411_LN_Leaf rep2, J4_LN_S_1: J411_LN_Seed rep1, J4_LN_S_2: J411_LN_Seed rep2.

c. Peak distributions in gene regions of different histone marks in the wheat genome.
d. Heatmaps of epigenetic marks for all annotated wheat genes which were sorted according to their expression levels determined by RNA-Seq.
e. Proportion of peaks located in TE regions for the six different histone marks.
f. H2A.Z profiles of DEGs that respond to external stimuli (abiotic and biotic stress); RNA-seq data from[27].
g. Fraction of bases for 15 states that vary between the different cultivars (top) and nitrogen availability (bottom).
h. Cross-correlation heatmaps of all H3K27me3 peaks which are located in distal or promoter regions separately. Abbreviations were as follow: KN_NN_R: KN9204_NN_Root, KN_NN_L: KN9204_NN_Leaf, KN_NN_S: KN9204_NN_Seed, KN_LN_R: KN9204_LN_Root, KN_LN_L: KN9204_LN_Leaf, KN_LN_S: KN9204_LN_Seed, J4_NN_R: J411_NN_Root, J4_NN_L: J411_NN_Leaf, J4_NN_S: J411_NN_Seed, J4_LN_R: J411_LN_Root, J4_LN_L: J411_LN_Leaf, J4_LN_S: J411_LN_Seed.

Fig. S2. Dynamic changes in the transcriptomes and epigenomes of NMGs

a. K-means clustering of LN-induced differentially-expressed NMGs in roots, leaves, and seeds. See also Supplemental Table 1. Abbreviations were as follow: NPF: NRT1/PTR FAMILY, NRT2: Nitrate transporter 2, CLC: Chloride channel protein, SLAH: Slow anion channel-associated homologues, AMT: Ammonium transporter, APC: The amino acid–polyamine–choline transporter superfamily, NIA: Nitrate reductase, NIR: Nitrite reductase, GS: Glutamine synthetase, GOGAT: Glutamate synthase, ASN: Asparagine synthetase, AspAT: Aspartate aminotransferase, GDH: Glutamate dehydrogenase, TF: transcription factor.
b. Percentage of NMGs in different categories marked by differential H3K27ac and H3K27me3. Abbreviations were same with (a).
c. H3K27ac levels of GS and GOGAT in the seeds of KN9204 and J411 between the two nitrogen availability levels (Wilcox test: ns: $p > 0.05$; *: $p \leq 0.05$; **: $p \leq 0.01$).
d. Representative tracks showing histone modifications and transcriptional changes of TaGS_2D in seeds for the two wheat cultivars and two nitrogen levels.
e. Grain protein content (GPC) in seeds of KN9204 and J411 under different nitrogen conditions (Student's t-test; ns: $p > 0.05$; *: $p \leq 0.05$).

Fig. S3. The functional influence of cultivar-biased H3K27ac peaks

a. Mean gene expression in J411 (x-axis) versus mean gene expression in KN9204 (y-axis) for genes associated with proximal cultivar-specific H3K27ac peaks separately in the leaf and seed.
b. Overlap between genes marked by cultivar-specific H3K27ac and DEGs between cultivars (blue circle) in the leaf (top panel) and seed (bottom panel) (Fisher's exact test was used to calculate the *p*-values for the overlaps).
c. GO enrichment of genes that are marked by proximal cultivar-specific H3K27ac peaks in KN9204 and J411.
d. Heatmaps showing the co-localization between cultivar-specific H3K27ac peaks and H3K4me3/H2A.Z.
e. Schematic diagram showing the approach used to link distal cultivar-specific H3K27ac peaks to genes.
f. Cross validation of distal cultivar-specific H3K27ac peaks assigned by Hi-C data.
g. Fraction of DEGs with distal KN9204-specific/J411-specific regulation (left) or DNA variation within the promoters located in QTLs (right) between KN9204 and J411. Abbreviation: Rt: root tip number; Rd: root diameter; Nup: Nitrogen uptake content; Nct: Nitrogen concentration; MRL: Maximum root length; TKW: Thousand-kernel weight; GPC: Grain protein content; Rs: Root surface area; Rdw: Root dry weight; Ls: flag leaf size.
h. Representative tracks of *TaXTH25* regulated by distal cultivar-specific H3K27ac peaks in *QMRL-7B*. Abbreviations were as follow: NN_R: NN_Root, LN_R: LN_Root.
i. Positive and negative control of luciferase reporter assay, region tested (positive: State5-8, negative: State5-10) got from data published before[32].

Fig. S4. Dynamic H3K27ac changes in KN9204 and J411

a. Heatmaps showing the differential H3K27ac peaks in the leaves and seeds of KN9204 and J411 under LN and NN conditions.
b. Peak distribution of differential H3K27ac peaks in roots, leaves, and seeds.
c. Dynamic H3K27ac and corresponding expression changes in the leaves of KN9204 and J411 seedlings. GO enrichments are shown on the right. Abbreviations were as follow: KN_NN_L: KN9204_NN_Leaf, KN_LN_L: KN9204_LN_Leaf, J4_NN_L: J411_NN_Leaf, J4_LN_L: J411_LN_Leaf.
d. Overlap between genes with up-regulated H3K27ac and the up-regulated DEGs for KN9204 and J411 in the seeds (Fisher's exact test was used to the calculate *p*-values for the overlaps).
e. Experiment design and western blotting of TSA (2 μM) treatment of KN9204 and J411 seedlings under the two nitrogen conditions. Abbreviations were as follow: KN_NN_R: KN9204_NN_Root, KN_LN_R: KN9204_LN_Root, J4_NN_R: J411_NN_Root, J4_LN_R: J411_LN_Root.

Fig. S5. Dynamic H3K27me3 changes in KN9204 and J411

a. Heatmaps showing the differential H3K27me3 peaks in seven clusters in the seeds of KN9204 and J411.
b. Distribution of differential H3K27me3 peaks in the roots and seeds.
c. Overlap between genes up-regulated for H3K27me3 and the down-regulated DEGs in the roots of KN9204 (Fisher's exact test was used to calculate the *p*-values for the overlaps).
d. Overlap between genes up-regulated for H3K27me3 and the down-regulated DEGs in the seeds of J411 (top panel) and KN9204 (bottom panel) (Fisher's exact test was used to calculate the *p*-values for the overlaps).

Fig. S6. The generation and influence to global H3K27me3 level of *Taswn-cr*

a. A phylogenetic tree showing the evolutionary relationships between Ez proteins (one part of PRC2) from *Arabidopsis* and wheat.
b. Expression of *TaSWN* and *TaCLF* genes under LN and NN conditions in KN9204 and J411.
c. DNA sequence identification the mutated target sites in the three *TaSWN* genes in the *Taswn-cr* mutant.
d. Peak numbers and lengths of H3K27me3 peaks in *Taswn-cr* and BW plants under different nitrogen conditions (Wilcox test: ns: $p > 0.05$; *: $p \leq 0.05$; **: $p \leq 0.01$; ***: $p \leq 0.001$; ****: $p \leq 0.0001$).
e. Profiles of H3K27me3 levels in *Taswn-cr* and BW under normal nitrogen conditions.
f. Peak distribution of the differential H3K27me3 peaks in Fig. 6a.
g. Overlap between genes marked by TaSWN-dependent H3K27me3 and genes marked by gain-H3K27me3 under LN condition in KN9204 (Fisher's exact test was used to calculate the *p*-values for the overlaps).

Figures

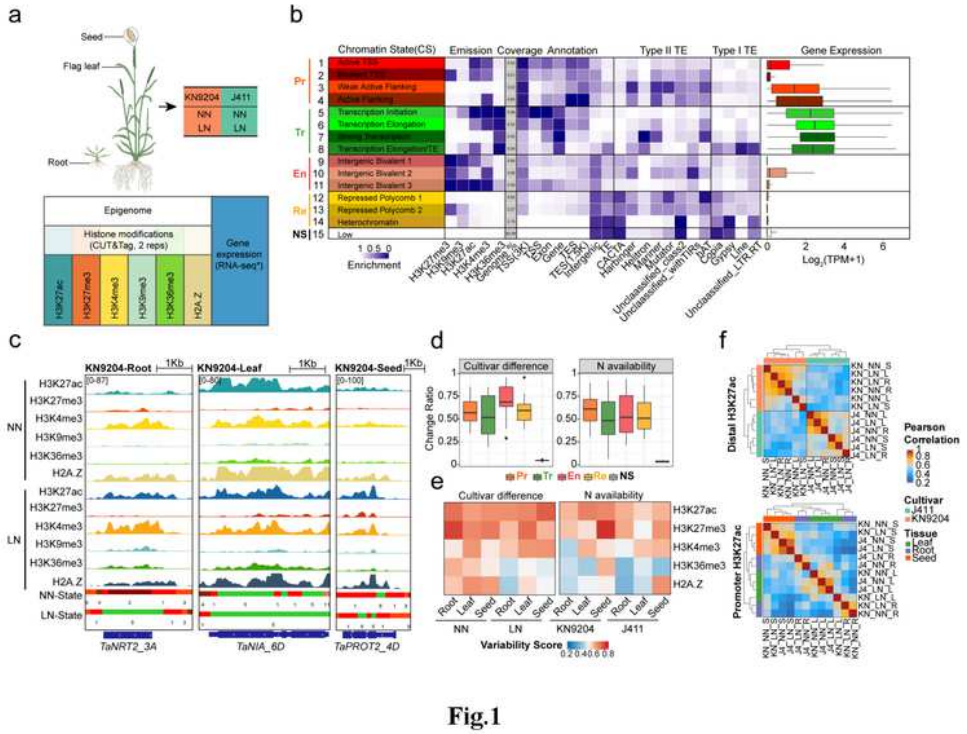

Fig.1

Figure 1

A 15-state model characterizes the dynamic chromatin landscape in KN9204 and J411

a. Experimental design for generating the epigenomic data sets in KN9204 and J411 under different nitrogen conditions.

b. Chromatin state definitions, genomic annotation enrichments, and expression levels of genes associated with each chromatin state. Chromatin states could be mainly organized into five categories: Pr (promoter), Tr (transcription), En (enhancer-like), Re (repressive), and Ns (No signal) states.

c. Schematic diagrams representing the chromatin state dynamics under different nitrogen conditions and tissues. State colors are as in (b).

d. The fractions of bases for the states of the five categories that vary between cultivar difference and nitrogen availability.

e. Variability scores of histone modifications between cultivar difference and nitrogen availability.

f. Cross-correlation heatmaps of all H3K27ac peaks which were located in the distal or promoter regions separately for the two cultivars and the two nitrogen conditions. Abbreviations were as follow: KN_NN_R: KN9204_NN_Root, KN_NN_L: KN9204_NN_Leaf, KN_NN_S: KN9204_NN_Seed, KN_LN_R: KN9204_LN_Root, KN_LN_L: KN9204_LN_Leaf, KN_LN_S: KN9204_LN_Seed, J4_NN_R: J411_NN_Root, J4_NN_L: J411_NN_Leaf, J4_NN_S: J411_NN_Seed, J4_LN_R:

J411_LN_Root, J4_LN_L: J411_LN_Leaf, J4_LN_S: J411_LN_Seed.

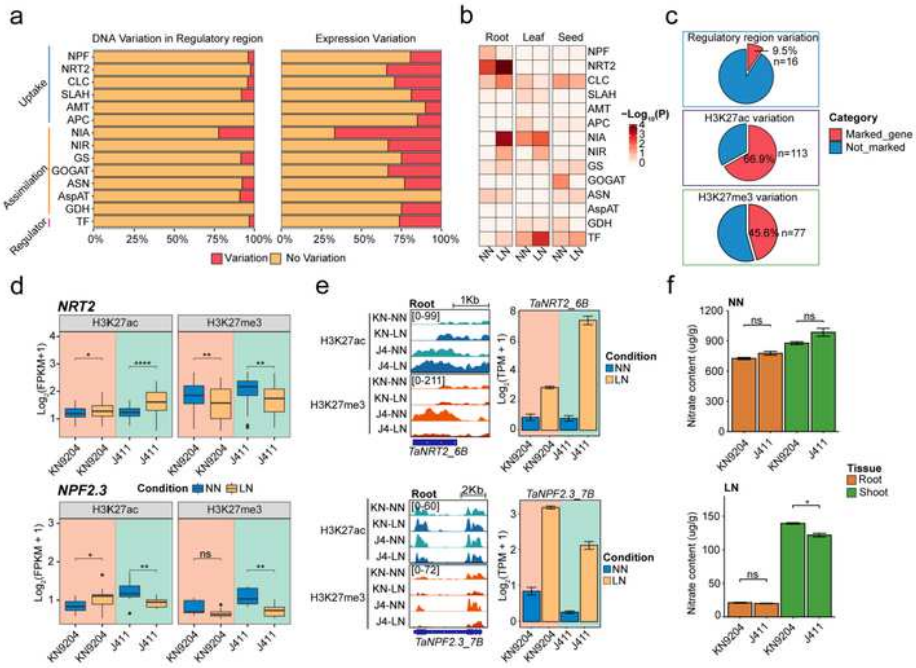

Fig.2

Figure 2

Epigenomic variations are vital to the expression bias of NMGs

a. Fraction of the regulatory regions and expression variation of nitrogen metabolism genes (NMGs) between wheat cultivars KN9204 and J411. Abbreviations were as follow: NPF: NRT1/PTR FAMILY, NRT2: Nitrate transporter 2, CLC: Chloride channel protein, SLAH: Slow anion channel-associated homologues,

AMT: Ammonium transporter, APC: The amino acid–polyamine–choline transporter superfamily, NIA: Nitrate reductase, NIR: Nitrite reductase, GS: Glutamine synthetase, GOGAT: Glutamate synthase, ASN: Asparagine synthetase, AspAT: Aspartate aminotransferase, GDH: Glutamate dehydrogenase, TF: transcription factor.

b. Enrichment of LN-induced differentially-expressed NMGs based on their functional category in three tissues (Fisher's exact test was used to calculate the p-values for the overlaps). Abbreviations were same with (a).

c. Proportion of NMGs showing expression variation between KN9204 and J411 with regulatory region variation (top panel), H3K27ac variation (middle panel), and H3K27me3 variation (bottom panel).

d. Histone modification (H3K27ac and H3K27me3) levels of NRT2 and NPF2.3 in the roots of KN9204 and J411 between the two nitrogen availability levels (Wilcox test: ns: $p > 0.05$; *: $p \leq 0.05$; **: $p \leq 0.01$; ****: $p \leq 0.0001$).

e. Representative tracks showing histone modifications and transcriptional changes of TaNRT2_6B and TaNPF2.3_7B in roots for the two wheat cultivars and two nitrogen levels.

f. Nitrate content of shoots and roots of KN9204 and J411 under two nitrogen conditions (Student's t-test; ns: $p > 0.05$; *: $p \leq 0.05$).

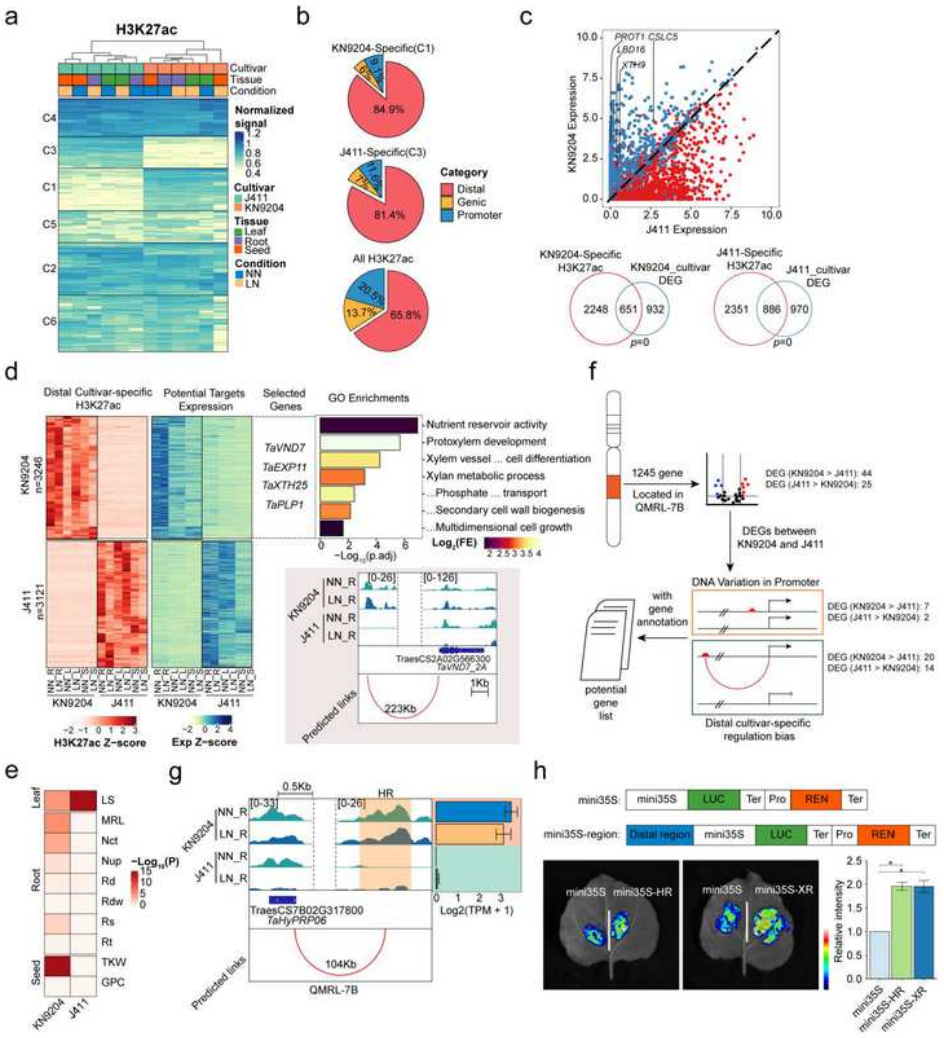

Fig.3

Figure 3

Distal regulatory region divergence is involved in NUE-trait variation between KN9204 and J411

a. K-means clustering of the variable H3K27ac peaks.

b. Peak distribution (distal, genic, or promoter) of cultivar-specific H3K27ac peaks in the wheat genome.

c. Mean gene expression in J411 (x-axis) versus mean gene expression in KN9204 (y-axis) for genes associated with proximal cultivar-biased H3K27ac peaks separately in the roots (top panel). Overlap between genes marked by cultivar-specific H3K27ac and DEGs between cultivars (blue circle) (bottom panel) (Fisher's exact test was used to calculate the p-values for the overlaps).

d. Assignment of distal cultivar-specific H3K27ac peaks to potential targets; representative genes and GO enrichment are shown on the right, and representative case is shown at the bottom. Abbreviations were as follow: NN_R: NN_Root, NN_L: NN_Leaf, NN_S: NN_Seed, LN_R: LN_Root, LN_L: LN_Leaf, LN_S: LN_Seed.

e. Enrichment of target genes with distal cultivar-specific H3K27ac peaks in QTLs between KN9204 and J411 (Fisher's exact test was used to calculate the p-values for the enrichment). Abbreviation: Rt: root tip number; Rd: root diameter; Nup: Nitrogen uptake content; Nct: Nitrogen concentration; MRL: Maximum root length; TKW: Thousand-kernel weight; GPC: Grain protein content; Rs: Root surface area; Rdw: Root dry weight; Ls: flag leaf size.

f. Schematic diagram illustrating the process used to narrow down potential key genes

regulated by distal cultivar-specific regulation in the QTL regions (QMRL-7B in this case).

g. Representative tracks of TaHyPRP06 regulated by distal cultivar-specific H3K27ac peaks in QMRL-7B. Abbreviations were as follow: NN_R: NN_Root, LN_R: LN_Root.

h. Luciferase reporter assay of cultivar-specific H3K27ac regions in track shown in (g) and Fig.S3.h (Student's t-test; ns: $p > 0.05$; *: p 0.05).

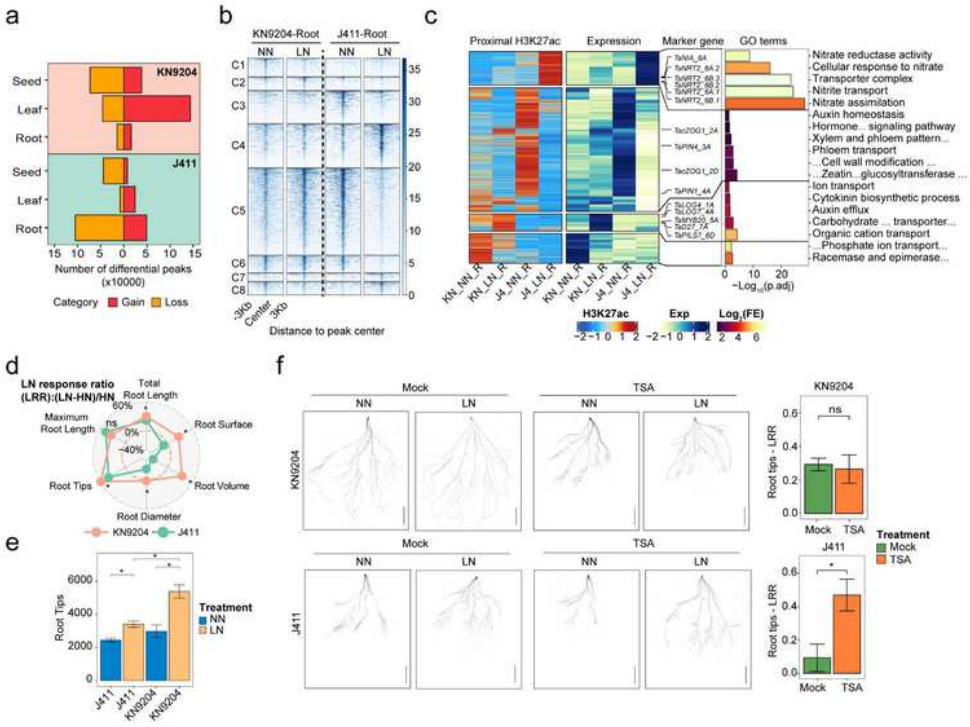

Fig.4

Figure 4

Dynamics of H3K27ac reveals the divergent strategies of KN9204 and J411 to low nitrogen conditions

a. The number of differential H3K27ac peaks in response to LN of three tissues (seeds, roots, leaves) in KN9204 and J411.

b. Heatmaps showing the differential H3K27ac peaks in eight clusters in the roots of KN9204 and J411 under NN and LN conditions.

c. Dynamic proximal H3K27ac peaks and corresponding gene expression changes in the roots of KN9204 and J411. Representative genes and GO (gene ontology) enrichments are shown on the right. Abbreviations were as follow: KN_NN_R: KN9204_NN_Root, KN_LN_R: KN9204_LN_Root, J4_NN_R: J411_NN_Root, J4_LN_R: J411_LN_Root.

d. The LN-response-ratio (LRR) of root systems for KN9204 and J411 (Student's t-test; ns: $p > 0.05$; *: $p \leq 0.05$).

e. The number of root tips in KN9204 and J411 plants under different nitrogen conditions (Student's t-test; ns: $p > 0.05$; *: $p \leq 0.05$).

f. Phenotypes of the root systems of KN9204 and J411 seedlings in the control (mock) and TSA treatments (2 μM) under different nitrogen conditions. Scale bars=5cm. The right panel is the LRR of the root tips (Student's t-test; ns: $p > 0.05$; *: $p \leq 0.05$).

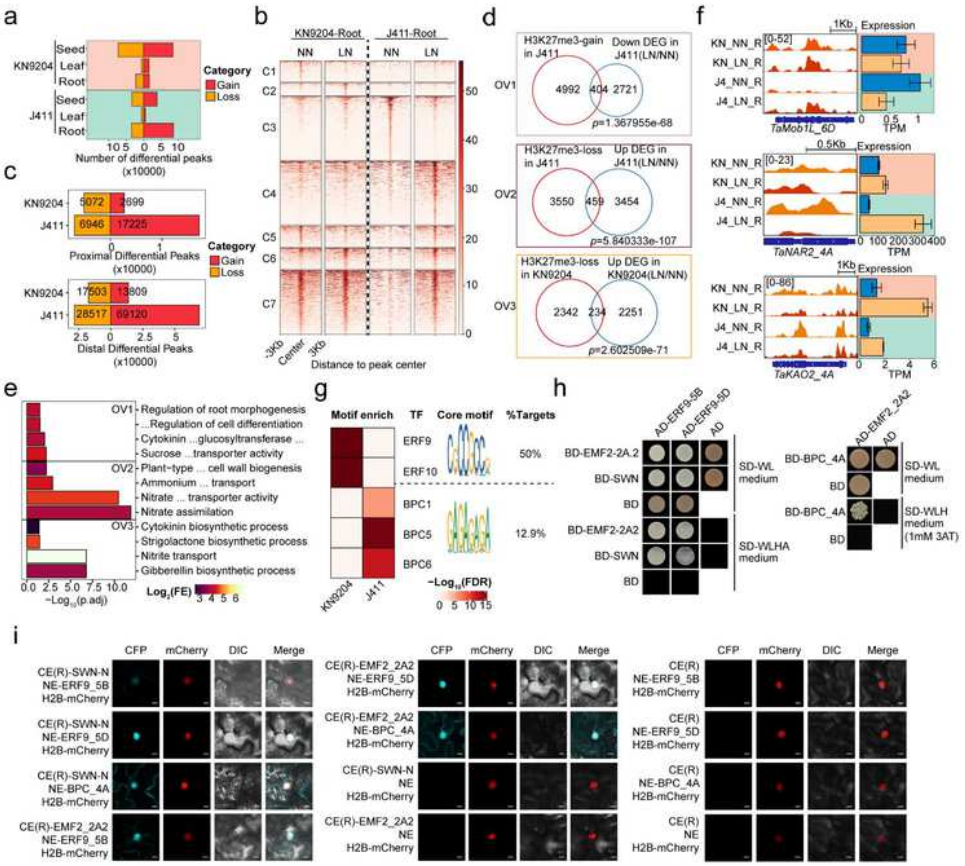

Fig.5

Figure 5

Different trends in H3K27me3 shapes adaptation bias between the cultivars KN9204 and J411

a. The number of differential (gain or loss) H3K27me3 peaks in response to LN of three tissues in KN9204 and J411.

b. Heatmaps showing the differential H3K27me3 peaks in the seven clusters in the roots of KN9204 and J411 under LN and NN conditions.

c. The number of differential H3K27me3 peaks (in proximal or distal regions) in the root of KN9204 and J411 plants in response to LN.

d. Overlap between genes with dynamic changes in H3K27me3 and DEGs in the roots (Fisher's exact test was used to calculate the p-values for the overlaps).

e. GO enrichment of the overlapping genes related to (d).

f. Representative tracks showing H3K27me3 and transcriptional changes in TaMob1L_6D (top panel), TaNAR2_4A (middle panel), and TaKAO2_4A (bottom panel) for the two cultivars under LN and NN. Abbreviations were as follow: KN_NN_R: KN9204_NN_Root, KN_LN_R: KN9204_LN_Root, J4_NN_R: J411_NN_Root, J4_LN_R: J411_LN_Root.

g. Sequence motif enrichment for the up-regulated H3K27me3 peaks under LN conditions in KN9204 and J411 (Fisher's exact test was used to calculate the p-values for the enrichment).

h. Yeast two-hybrid (Y2H) assays showing the interaction between TaERF9_5B/TaERF9_5D/TaBPC_4A and TaEMF2-2A.2/TaSWN (components of PRC2).

Transformed yeast cells were grown on synthetic media lacking Leu and Trp (-WL) and Leu, Trp, His, and Ade (-WLHA) or Leu, Trp, and His (-WLH) with 1mM 3AT.

i. BiFC analysis of the interaction between TaERF9_5B/TaERF9_5D/TaBPC_4A and TaSWN-N/TaEMF2_2A.2. Scale bars = 10 mm.

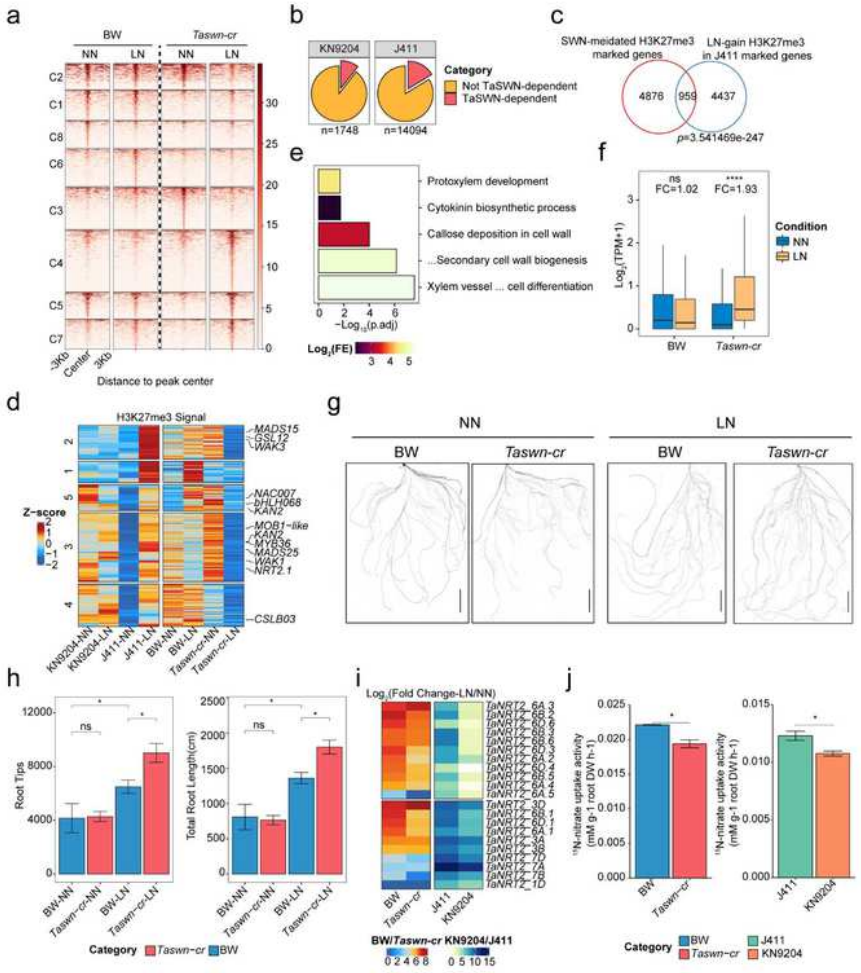

Fig.6

Figure 6

Rewiring H3K27me3 strengthens root adaptation to low nitrogen fertilization level

a. Heatmaps showing the differential H3K27me3 peaks in ‘BobWhite’ (BW) and the Taswn-cr mutant plants in the eight clusters under NN and LN conditions.

b. The proportion of TaSWN-dependent peaks in the up-regulated H3K27me3 peaks under LN conditions in KN9204 and J411.

c. Overlap between genes marked by TaSWN-dependent H3K27me3 and marked by gain-of-H3K27me3 under LN conditions in J411 (Fisher's exact test was used to calculate the p-values for the overlap).

d. Dynamic changes in the TaSWN-dependent H3K27me3 peaks under different nitrogen conditions (NN and LN) in KN9204, J411, BW, and Taswn-cr plants. Representative gene names are shown on the right.

e. GO enrichment of the overlapping genes related to (d).

f. The expression changes and fold-changes of the genes in (d). (Wilcoxon test: ns: $p > 0.05$; ****: $p \leq 0.0001$) FC: fold-change.

g. Scans of root systems of BW and Taswn-cr seedlings grown under different nitrogen conditions. Scale bars = 5 cm.

h. The number of root tips and total length of the root systems for BW and Taswn-cr seedlings grown under different nitrogen conditions. (Student's t-test; ns: $p > 0.05$; *: $p \leq 0.05$).

i. The fold-changes in the expression of NRT2 genes in BW, Taswn-cr, J411, and KN9204 seedlings grown under different nitrogen conditions.

j. 15N-nitrate uptake activity of different seedlings (KN9204, J411, BW, and Taswn-cr) grown under LN conditions (Student's t-test; ns: $p > 0.05$; *: $p \leq 0.05$).

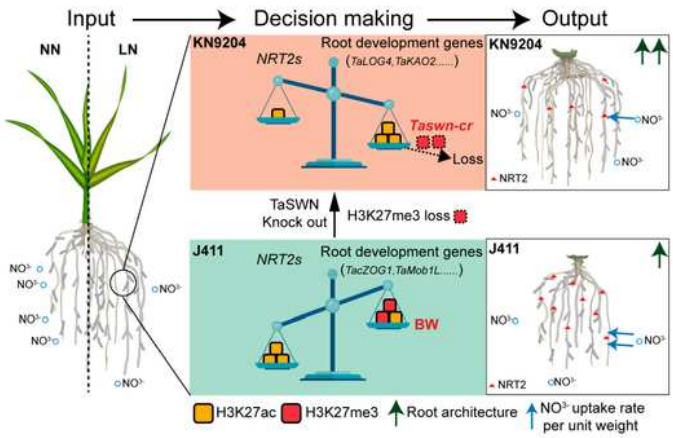

Fig.7

Figure 7

The balanced model of epigenetic regulation for divergent strategies to LN conditions in wheat

In the low-nitrogen condition (Input, left), different adaptation strategy of wheat is selected from the balance between root system development and nitrate uptake transporters (NRT2s). great gain-of-H3K27ac enhance the expression of root development-related genes in KN9204, Conversely, greater gain-

of-H3K27me3 and minor gain-of-H3K27ac reduce root development in J411, but with an associated increase in nitrate uptake transporters (NRT2s) via gain-of-H3K27ac. After the knock-out of TaSWN (Taswn-cr), there is de-repression of root development, accompanied by the loss of H3K27me3 (Decision making, middle). Phenotypically, KN9204 has a developed root architecture (higher expression of root development genes) but lower nitrate uptake rate per unit weight (lower expression of NRT2s). In contrast, J411 has a diverse selection with regards to this balance (Output, right).

Supplementary Files

This is a list of supplementary files associated with this preprint. Click to download.

- TableS1DifferentialexpressionandhistonemodificationsofNMGs.xlsx
- TableS2Cultivarspecificregulation.xlsx
- TableS3ERFinQTL.xlsx
- TableS4Primerusedinthisstudy.xlsx
- NCOMMS2315670RS.pdf